Republic of Iraq
Ministry of Higher Education & Scientific Research
University of Babylon
College of education for pure sciences
Department of Physics

Scattering Reactions Mechanism of Some Stable and Unstable Nuclei on Medium and Heavy Mass Targets

A Thesis

Submitted to the council of the College of Education for Pure Sciences of University of Babylon in Partial Fulfillment of the Requirements for the Degree of Master in Education / Physics

By

Zainab Hafedh Mousa Sabeel

B. Sc. in Physics

(University of Babylon, 2009)

Supervised by

Dr. Fatima Mohammad Hussain (Ph.D.)

College of Education for Pure Sciences

Department of Physics

2022 A.D. **1444 A.H**

(سورة المجادلة)

(الآية 11)

Supervisor certificate

I certify that this thesis entitled **"Scattering Reactions Mechanism of Some Stable and Unstable Nuclei on Medium and Heavy Mass Targets"** is prepared by the student **(Zainab Hafedh Mousa Sabeel)** under my supervision at the College of Education for Pure Sciences, University of Babylon as partial fulfillment of the requirement for the Degree of Master in Education / Physics.

Signature:
Name: Dr. Fatima M. Hussain
Title: Assistant Professor
(Supervisor)
Date: / / 2022

Head of the Department Certificate

In view of the available recommendations, I forward this thesis for debate by the examining committee.

Signature:
Name: Dr. Khalid H. Abbas
Title: Professor
(Head of Physics Department)
Date: / / 2022

Scientific Supervisor's Certification

This is to certify that I have read this thesis entitled **"Scattering Reactions Mechanism of Some Stable and Unstable Nuclei on Medium and Heavy Mass Targets"** and I found it is qualified for debate.

Signature:

Name: Dr. Ali Abid Abojassim

Title: Professor

Address: University of Kufa

Date: / / 2022

Scientific Supervisor's Certification

This is to certify that I have read this thesis entitled **"Scattering Reactions Mechanism of Some Stable and Unstable Nuclei on Medium and Heavy Mass Targets"** and I found it is qualified for debate.

Signature:

Name: Dr. Rawaa Mezher Obaid Ashoor

Title: Assistant Professor

Address: University of Babylon

Date: / / 2022

Linguistic Supervisor's Certification

This is to certify that I have read this thesis entitled **"Scattering Reactions Mechanism of Some Stable and Unstable Nuclei on Medium and Heavy Mass Targets"** and I found it is qualified for debate.

Signature:

Name: Dr. Ahmed Rawdhan Salman

Title: Assistant Professor

Address: University of Babylon

Date: / / 2022

Examining Committee Certification

We certify that we have read the thesis entitled **"Scattering Reactions Mechanism of Some Stable and Unstable Nuclei on Medium and Heavy Mass Targets"** and as a committee examined the student in its contents and, according to our opinion, it is accepted as a thesis for the Degree of Master in Education / Physics.

Signature:
Name: Dr. Fouad Attia Majeed
Title: Professor
Date: / / 2022
(Chairman)

Signature:
Name: Dr. Inaam Hani Khadim
Title: Assistant Professor
Date: / / 2022
(Member)

Signature:
Name: Dr. Adil Jalel Najim
Title: Lecturer
Date: / / 2022
(Member)

Signature:
Name: Dr. Fatima Mohammed Hussain
Title: Assist professor
Date: / / 2022
(Member and Supervisor)

Approved by the dean of the college committee for post Graduate studies

Signature:
Name: Dr. Bahaa Hussein Rabee
Title: Professor
Address: Dean of the College of Education for Pure Sciences
Date: / / 2022

Dedication

This thesis work is dedicated to:

My father

My mother

My husband

My brothers and sisters

My friends

For their support and encouragement ...

Acknowledgements

Praise be to Allah lord of the whole creation, who gave me health and strength to carry out the present research.

Then, I would like to thank my supervisor, **Dr. Fatima Mohammad Hussain** for the countless hours that she dedicated to this thesis. Her expertise in this field greatly improved the contents of this thesis. I am grateful for her helpful comments, suggestions and constructive criticism throughout this project. My thesis has benefited substantially from her insightful recommendations.

A word of thanks is due to the staff members of the Department of Physics in the College of Education for Pure Sciences and to the Dean of the College of Education for Pure Sciences at the University of Babylon for their help and kind assistance.

It gives me immense pleasure to thank **Mr. Yousif Abdul-Hakeem Abdul-Hussein** from the Department of Physics of the College of Education for Pure Sciences, for his assistance, which has always played a key role in the scientific developments of the present thesis, and his support during the development of all the programming codes of this thesis, wishing him endless success in his life.

I am grateful to my family for their constant love and support. Thanks for their understanding, never-ending encouragement, and support throughout this work.

Zainab

Abstract

In this thesis, the scattering mechanism has been investigated by calculating the cross-sections of total (σ_T/σ_R) or elastic (σ_{el}/σ_R) scattering to Rutherford cross section and distribution (D_{el} or D_T) (MeV^{-1}) of Coulomb barrier for the stable and unstable nuclei of several systems, which are: $^{6}He+^{208}Pb$, $^{17}F+^{208}Pb$, $^{7}Be+^{58}Ni$, $^{7}Li+^{59}Co$, $^{6}Li+^{59}Co$, $^{16}O+^{64}Zn$, $^{32}S+^{208}Pb$, and $^{11}Be+^{209}Bi$.

The nuclear potential is taken to be the Wood-Saxon (WS) potential which contains the parameters of the real and imaginary part which are depth, radius and nuclear surface diffusion coefficient. The best values of parameters of the optical potential were implemented by a good fit of the theoretical calculations with the measured values of the scattering cross sections. This study is based on the theory of Alder and Winther (AW) which was originally proposed to treat the Coulomb excitation of nuclei which is called Continuum-Discretized Coupled Channels (CDCC) method.

The coupling of reaction channels with breakup channel on the calculations have been implemented by the CC-SCT programmed code represents the latest version of the full quantum mechanics CC code that was programmed in Fortran language. A sub-program has been written by Fortran language to calculate the scattering barrier distribution D_{el} or D_T using the numerical two-point-difference method. This sub-program has been implemented in CC-SCT code for theory and measured results.

The calculations of the ratio between the scattering cross-sections to the Rutherford scattering sections as a function of the center of the angle θ_{cm} and a function of the center of the energy E_{cm} in addition to calculating the scattering distribution as a function energy in cases of coupling and non-coupling. All calculations in good agreement with observed values.

Contents

List of Figures

List of Tables

List of Symbols

Symbol	Physical Meanings
α	Alpha particle
a_0	Diffuseness parameter
a	Projectile nucleus
A_P, A_T	Mass number of projectile and target nuclei
AW	Alder-Winther theory
CC	Coupled Channel
CDCC	Continuum Discretized Coupled Channel formalism
CRC	Coupled Reaction Channel
DF	Double folding
E_{lab}	Energy in the laboratory system
OM	Optical model
p	Proton
R_B	Position of the Coulomb barrier
R_C	Radius of system charge sphere
r_0	Radius parameter

SC	Single Channel
S_l	Nuclear *S*-matrix
V(r)	Interaction Potential
V_0	Nuclear potential depth
V_b	Coulomb barrier height
V_C	Coulomb potential
V_N	nuclear potential
WS	Wood-Saxon
X	Target nucleus
Z_P, Z_T	Atomic number for projectile and target nuclei
$f_C(\theta, \phi)$	Coulomb scattering amplitude
$f_N(\theta, \phi)$	Nuclear scattering amplitude
$\frac{d\sigma_{el}}{d\Omega}$	Elastic scattering differential cross sections
$\frac{d\sigma_{in}}{d\Omega}$	Inelastic scattering differential cross sections
$\frac{d\sigma_T}{d\Omega}$	Total scattering differential cross sections
$\frac{d\sigma_R}{d\Omega}$	Rutherford scattering differential cross sections
T	Kinetic energy operator of the relative motion between the projectile and target nuclei
∇^2	Laplace operator

U	Interaction potential in coupled channels
H	Coupled channels Hamiltonian
H_0	Intrinsic Hamiltonian
$\|\eta\rangle$	Eigenstates of the intrinsic Hamiltonian
δ	Kronecker delta
e_η	Eigenvalue of intrinsic energy
U'	Diagonal part of interaction potential in coupled channels
η_S	Somerfield coefficient
U''	Non-diagonal part of interaction potential in coupled channels
τ	Intrinsic coordinates
β^-	- ev beta decay
β^+	+ ev beta decay
σ_{el}	Elastic scattering cross sections
σ_T	Totel scattering cross sections
D_{el}	Elastic scattering barrier distribution
D_T	Total scattering barrier distribution
$\Psi(\vec{r})$ or $\psi^{(+)}(\vec{r})$	Total scattered wave function
ℓ or λ_C	angular momentum

$\hbar$	Blank reduced constant
E	Total energy
e	Absolute electron charge
R_0	Radius of nuclear potential
U^{opt}	Complex potential in optical model
V^{opt}	Real part of complex potential in optical model
W^{opt}	Imaginary part of complex potential in optical model
$E_{c.m.}$	Energy center of mass
$\theta_{c.m.}$	Scattering angle center of mass
$d\Omega$	Solid-angle element
μ	Reduced mass
$\vec{k}$	Incident wave vector
θ	Polar angle
ϕ	Azimuthal angle
r_C	Coulomb's turning point
$R_0(E)$	Probability of reflection
$T_0(E)$	Probability of transmission
$\hbar\Omega$	Coulomb barrier curvature

ϕ_c	Wave function for pure Coulomb scattering
σ_R	Rutherford cross section
$\left\|\Psi_\eta\left(\eta_0, \vec{k}_0\right)\right\rangle$	Eigenstate of all order coupled channels
$\left\|\psi_\eta\left(\eta_0, \vec{k}_0\right)\right\rangle$	Eigenstate of one order coupled channels
T_η	Transmission coefficients
$H_\ell^{(-)}, H_\ell^{(+)}$	Hankel functions
σ_{el}^{cl}	Scattering cross sections pure classical approach

Chapter One

General Introduction

1.1 Introduction

Elastic scattering and reaction mechanisms around the barrier in collisions induced by halo nuclei have been the object of many publications in recent years in an attempt to investigate both the effect of the projectile halo structure and the effect of break-up coupling on the dynamics of the reaction. Hundred years later [1], Rutherford's alpha (α) scattering elastic scattering experiment turned out to be a very useful tool for studying unusual nuclear structures like the nuclear halo for example. Because elastic scattering is a peripheral method, it can provide information on the tail of the wave function and therefore you can learn about surface properties such as nuclei sizes and surface diffuseness and how they can influence the shape of the projectile target [1].

Total scattering can be calculated as the sum of the elastic scattering, the inelastic scattering and the transfer reaction. The fusion reaction is also very well comparable, which is characterized as a reaction in which two distinctive nuclei merge together to form a composite system. Fusion and total scattering are both known to be comprehensive operations and complement each other [2]. As a result, both interactions are subject to the same potential and share the same knowledge about the interaction mechanism, and both are sensitive to the impacts of channel coupling (due to mutual inelastic excitations of the colliding nuclei) at energies near the Coulomb barrier. Nucleus on ^{64}Zn near the barrier [2].

The analysis of the first experiments on the interaction of the He, Li, and Be neutron-rich isotopes with stable target nuclei has led to the assumption that on these nuclei, there is a long tail distribution of nucleon density, arising from the low binding energy of the outer nucleons [3].

Understanding the potential of two colliding nuclei is of a fundamental importance for explaining collisions between nucleus-nucleus. The nucleus-nucleus potential is the sum of an attractive short-range nuclear potential $V_N(r)$

and potential $V_C(r)$ along range repulsive Coulomb. This was shown by the exact description of the Coulomb or Rutherford scattering, the scattering where only Coulomb is long-range potential works. The exact form of the attractive potential between two nuclei is not well understood, except for Coulomb potential. One way to determine the nuclear potential is to accept some form of it, and to determine the parameters to replicate the experimental data. The most commonly used phenomenological form of Woods-Saxon defined by the parameter of radius, the potential depth, and the parameter of surface diffuseness. The major advantage is that it is simple which will make it easier to perform theoretical calculations. Experimental data can be analyzed on the nuclear potential by fusion or total scattering. At zero impact (i.e., head-on collision), scattering is relevant to the probability of reflection of the potential barrier, whilst fusion is due to the possibility of penetration. Technically, true, the scattering cross-sections cannot be investigated experimentally at a deflection angle of 180° [4]. Nevertheless, it has shown that the wide-angle scattering can be estimated as scattering at the zero-impact parameter via centrifugal correction where scattering is probable to become more appropriate but less error-prone than fusion experiment results [4].

Many interesting phenomena can happen in the heavy-ion collisions. For instance, by choosing targets and projectiles properly, various degrees of freedom in the nuclei can be excited in particular; These are related to the one-particle motion and the collective motion. The investigation of the isolated zone where nuclei are stable in the island of stability too contributed to the configuration of several super-heavy elements, which are not present in nature [5]. With regard to a nuclear potential, the nuclear potential parameters for heavy ion systems taken directly from fusion experimental data vary from that are used for total scattering experimental data [6], as well as this is still not well understood. It seems, thus, that further analyzes of the nuclear potential for heavy-ion collisions, which could be single from the nuclear potential for light-ion collisions, and intended to make

further progress in the knowledge of heavy-ion reactions. The collision nucleus should be placed close to each other to explore the nuclear potential in such a manner that the nuclear power of one nucleus is experienced by the other nucleus. Hence, at energies close enough to the height of the Coulomb barrier, the nucleus will collide. Along the height of the Coulomb barrier, it has been well known, for example, that the internal structures of the colliding nucleus play an important role, that the coupling to mutual excitations, such as rotational and vibrational states, has been demonstrated [2].

In recent decades, heavy-ion total scattering and fusion reactions at energies which are close to the Coulomb barrier have been extensively researched, offering an excellent opportunity to obtain details about the nuclear structure and nucleus-nucleus interaction and to investigate the mechanism of heavy-ion reactions at near-barrier energies of great significance for the synthesis of super-heavy energies [7]. Based on the principle of quantum tunneling, total scattering (a collection of elastic, inelastic scattering and transfer channels) is known to be a strong equivalent of the fusion reaction in the sense that the former is related to the probability of a potential barrier being expressed while the latter is related to the probability of penetration. It has also been shown that the fusion barrier distribution produced by coupling the relative motion of the nuclei to internal degrees of freedom can be obtained from the carefully measured excitation functions for fusion [7].

Scattering of heavy-ion at reverse angles is a counterpart to a heavy-ion reaction to fusion. These are inclusive operations that are prone to channel coupling effects at energies close to the Coulomb barrier (due to collective inelastic excitations of the colliding nuclei). A main difference is that the total scattering is due to the Coulomb barrier's probability of reflection, whilst transmission is related to the fusion. Taking advantage of this truth, barrier distributions were obtained [8].

An additional significant informant of knowledge on the density distribution of matter in halo nuclei is given by the elastic scattering in experimental analyses of the properties of these exotic nuclear systems, along with methods of separation, breakup, and nucleon transfer, etc. It should be observed that the conditions of an experiment involving the inclusion of halo nuclei are often such that a distinction is not created between the contributions of the elastic and inelastic processes when the particles are registered [3].

One should take into consideration that no experiment directly measures the barrier of a reaction. For all the experiments involving the fusion and scattering processes, one also measures the differential cross-sections and then can obtain barrier parameters using an acceptable theoretical method. several authors used bare ability to extract barrier parameters according to Akyüz-Winther (AW) [9].

1.2 Scattering Technique

The most important experimental technique in quantum physics is the scattering experiment. Where in nuclear physics, the first clear evidence of nuclear structure came from Rutherford's observation of the scattering reaction. The theoretical tool for the analysis of scattering experiments is scattering theory. Scattering theory is the study of an interacting system on a time and/or distance scale which is large compared to the scale of the actual interaction [10, 11]. In general, the results of a nuclear collision may be one of a number of possible reactions, each one of which sheds light on a particular aspect of nuclear structure or nuclear behavior. Research scientists measure different reactions in order to study the nuclear force, synthesize new nuclei, determine nuclear size and shapes and investigate the properties of excited nuclei. According to the classical picture, the projectile can induce various kinds of reactions depending on the impact parameter or the corresponding angular momentum and the dynamical behavior

of nuclear matter during different types of collision in the classical picture of HI as shown in Fig. (1.1) [12-14].

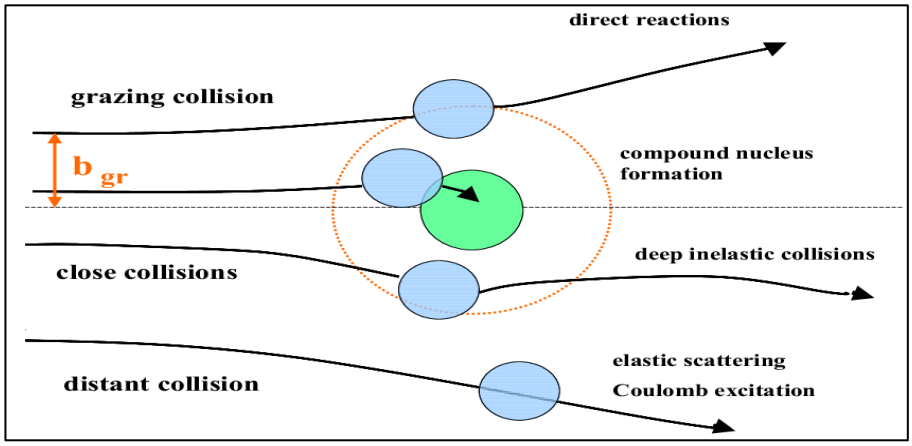

Figure 1.1: Distant, grazing and close collisions in the classical picture of heavy ion collisions [15].

1.3 Types of scattering reactions

1.3.1 Elastic Scattering

In this type of reaction, the target nucleus (X) is left in its ground state, there is no change in the potential energy, and of course the projectile and target are the same. The only difference is that the kinetic energy of the target will be less than that of the projectile [16-18], the general representation of this type of reaction is:

$$X(a,a)X$$

1.3.2 Inelastic scattering

Inelastic scattering is the process by which, the target nucleus is left in an excited state, i.e. both projectile and target are kept their identity, except that the product nucleus is in an excited state with respect to the target which be in the ground state [16-18], the general representation of this type of reaction is:

$$X(a,a)X^{*}$$

1.3.3 Transfer Reactions

In transfer reactions, when the projectile passes over the periphery of the target, one or more nucleons are transferred between the projectile and the target, such as an incoming deuteron turning into an outgoing proton or neutron, thereby adding some nucleons to the target A to form a nucleus, B [19].

1.3.4 Deep Inelastic Scattering

This reaction entails substantial damping of kinetic energy and mass exchange. The larger fragments are highly deformed and excited while retaining partial memory of target and projectile masses and charges. This process takes place at energies above the Coulomb barrier [12, 19].

1.4 Nuclear structure and exotic nuclei

The chart of nuclides (Fig. 1.2) is a good starting point for any discussion of nuclear structure. Nuclei consist of a certain number of nucleon-protons and neutrons are arranged in this chart accordingly. An arrangement of protons alone would be unbound, due to the coulomb repulsion between the positively charged particles [20]. The attractive nuclear force acts between nucleons and can counterbalance the effect of the Coulomb force to break apart the nucleus. A bound or stable nucleus has the correct number of protons and neutrons such that the repulsive coulomb force is overcome. These are the nuclei that appear as the backbone of the chart of nuclei, forming what is known as the valley of stability [21].

One of the first and most useful models of nuclear structure is the Shell model [22]. This idea began with the striking observation of magic nuclei - especially stable nuclei with proton and/or neutron numbers equal to 2, 8, 20, 28, 50, 82 and 126 - which indicated a shell structure analogous to that of atomic electron configurations. Such behavior would not be reproduced by a liquid drop

model, for example. The challenge was then to find an adequate potential for the system of nucleons which would at the very least reproduce the observed magic numbers. This was finally done in 1950 when the spin orbit interaction, whose contribution had been somewhat underestimated, was included [23].

Modern shell model calculations account for interactions between nucleons in different orbitals, but the model space can be so large for heavy nuclei that an assumption of an inert core at some level must be made to have a workable model space.

Stable nuclei are for obvious reasons more easily studied. Therefore, the refinement of the shell model potentials for example, has been biased towards the valley of stability. In predicting the structure of these nuclei, our theories are well matured. However, for exotic nuclei away from stability, this is also of interest [24].

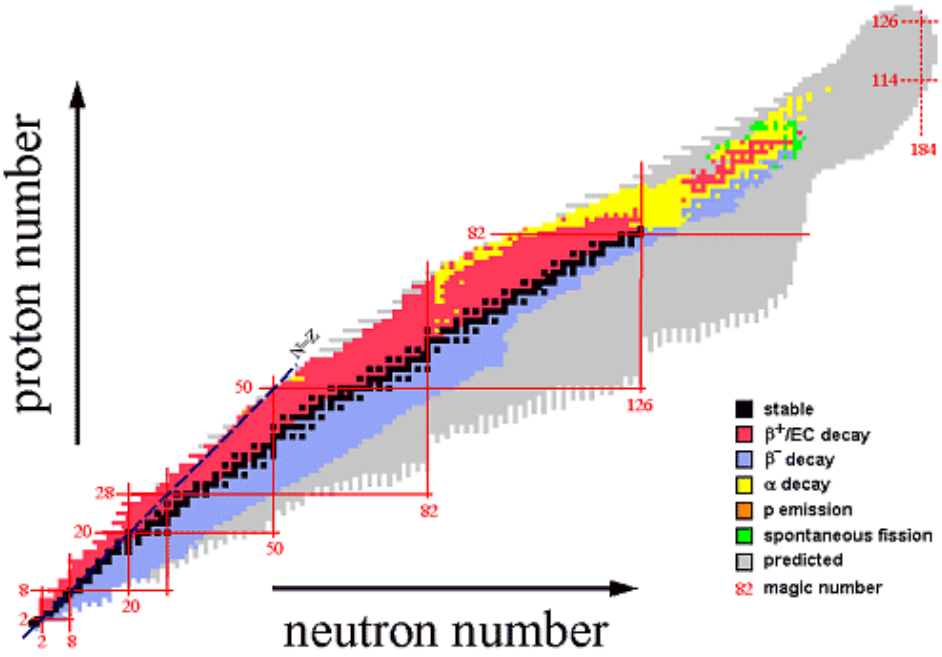

Figure 1.2: Chart of nuclides. Stable nuclides are shown in black, at the bottom of the so called "Valley of Stability" in the nuclear landscape. Unstable nuclei that decay predominantly via β^+ decay or eletron capture are shown in red, and by β^- decay in blue. Unknown nuclei (not yet studied experimentally) are shown in grey up to the predicted limits of nuclear existence the proton and neutron drip lines. Fission nuclei are shown in green and only appear at heavier masses [25].

Exotic nuclei are nuclei with an unusual proton to neutron ratio. They can be either rich or poor in neutrons compared to their stable isotopes at the line of stability. Such nuclei will typically undergo beta decay back towards more tightly bound nuclei at the bottom of the valley of stability. This makes them short-lived and therefore difficult to produce and study [26].

As experimental techniques have matured, we have become able to produce and study increasingly exotic nuclei. Not surprisingly, predictions of the shell structure of these nuclei with models that were obtained from data at stability have had limited success. Several unexpected phenomena have emerged, and will surely help to better the understanding of nuclear structure [27].

The study of deformation and collective behaviours of non-spherical nuclei is of equal importance. The most striking example thereof is in the neutron deficient Pb isotopes, where Shape Coexistence [28], the competition of different shapes at comparable energies is clearly observed. This phenomenon has been observed across the nuclear landscape, but due to difficulties in producing exotic nuclei, is not too well studied in the very neutron poor Pb isotopes where it appears to be strongest [28].

Studies of the interaction between nucleons in exotic nuclei will also aid in its understanding.

To summarize - the systematic study of exotic nuclei is important for three main reasons [28]:

1. To test, refine and develop models for nuclear structure by acquiring new data. This data is also useful for astrophysical calculations and predictions.
2. Exploration; to discover new behaviours and understand their consequences for theoretical pictures.
3. To determine the limits of nuclear existence by studying nuclei at the drip lines.

1.5 Literature review

There are many researches studies close to the current study and they are some to be mentioned here:

In 2000, S. V. S. Sastry and S. Santra [29] explained the Coupled Reaction Channel (CRC) was used because these channels have a major impact on the fusion's excitation function. Elastic and total pathways, on the other hand, will unambiguously restore the structure and the reaction in a parallel analysis of the fusion. The fusion excitation functions for the ^{16}O + ^{208}Pb method, for example, are equipped with the same fusion barrier distributions for nuclei with different structures.

In 2001, S. Santra *et al.* [30] measured elastic, inelastic, and transfer angular distributions for $^{12}C+^{208}Pb$ in the energy range from 58.9 to 84.9 MeV. While the fission fragment angular distributions were measured over the energy range from 58.9 to 79 MeV. The effective nucleus-nucleus real potential, obtained from CRC calculations, explained the observed energy dependence of the real part of the optical potential. Thus, the real potential used in these calculations with such a large number of constraints can be considered as the bare nucleus-nucleus potential.

In 2002, T. J. Schuck *et al.* [31] evaluated total scattering data back ward angles for the systems $^{34,32}S+^{197}Au$ and $^{34,32}S+^{208}Pb$ for energies spanning the Coulomb barrier have been extracted from the data. For the fusion reactions of $^{34,32}S$ with ^{197}Au.

In 2003, I. Gontchar *et al.* [32] shown that in order to balance the experimental results for ^{16}O + ^{208}Pb and $^{12}S+$ ^{208}Pb structures, the Woods-Saxon (WS) potential diffusion parameters must be equal to 1fm for the over barrier energies and fusion cross-sections. These diffuseness parameter values were high

when compared to elastic scattering values. The nucleus-nucleus potential was calculated using the double folding model, which was used to estimate fusion barrier energies and nuclear potential diffusion.

In 2004, A. Pakou *et al.* [33] studied the $^{7}Li+^{28}Si$ elastic scattering at near-barrier energies, with the aim to map the real and imaginary part of the optical potential and therefore probe the threshold anomaly. For a better understanding of our results, continuum-discretized-coupled-channel calculations were also performed and are discussed.

In 2005, R. C. Johnson [34] described adiabatic approximations to few-body models of nuclear scattering with emphasis on reactions with deuterons and halo nuclei (frozen halo approximation) as projectiles. The different ways the approximation should be implemented in a consistent theory of elastic scattering, stripping and break-up are explained and the conditions for the theory's validity are briefly discussed. A formalism which links few-body models and the underlying many-body system is outlined and the connection between the adiabatic and CDCC methods is reviewed.

In 2006, K. Washiyama *et al.* [35] discussed nuclear potential for a Woods-Saxon, it was inferred that a high value of the surface diffuseness parameter was used, is a successful fusion reaction comparable using large-angle total scattering to explore the possible ingredients that are missing from existing nuclear reaction models and to clarify the obvious inconsistency in the diffuseness parameter for fusion reactions.

In 2007, K. Hagino [36] showed that the surface diffuseness parameter of the nucleus-nucleus potential was calculated using total scattering of deep-sub barrier energies, and coupling channels for total scattering barrier distribution were investigated for the $^{70}Zn +^{208}Pb$ reaction. The coupling-channel equations, which include multi-phonon excitations in the collisioning nuclei, demonstrate

that the experimental excitation process for reverse angle total scattering and the barrier distribution for this reaction are reasonably well reproduced.

In 2008, N. Wang, and W. Scheid [37] studied fusion reactions, elastic and large-angle total scattering reactions with the same nuclear nucleus potential proposed. The elastic distribution angle distributions of many reactions are replicated relatively well by the proposed Woods-Saxon potential with fixed energy parameters far higher than the Coulomb barrier. The determined total scattering cross sections of a series of reactions are in good agreement with the experimental results, with an empirical barrier distribution based on the modified Woods-Saxon potential and taking into account the effect of nucleon transfer.

In 2009, K. Hagino [38] showed the lowest barrier in the barrier distribution to be regulated by fusion cross sections at deep sub barrier energies, and the surface region of the inter nuclear potential is determined using total scattering at deep sub barrier energies, while the inner component is calculated using the Semiclassical formula. They used this method to study the reactions $^{16}O + ^{144}Sm$ and $^{16}O + ^{208}Pb$.

In 2010, A. Izadpanah [39] performed the optical model analysis of the alpha particle elastic scattering on a carbon target on the basis of the dispersion relation between the real and imaginary parts of the calculated volume integrals. A nuclear dispersion anomaly in an $\alpha+^{12}C$ system was observed and interpreted clearly.

In 2011, W. H. Long and C. A. Bertulani [40] studied the nucleus-nucleus interaction potential within the relativistic mean field theory. The systematics of the relativistic effects have been investigated by analyzing the relation between the potential and the bombarding energy as a function of the impact parameter. It is shown that the potential barriers are noticeably sensitive to the bombarding energy for a given impact parameter. At large bombarding

energies the slope at the potential edge decreases with the impact parameter. Comparisons with a non-relativistic treatment shows that relativistic effects cannot be ignored at bombarding energies around and larger than 100 MeV/nucleon.

In 2012, V. Scuderi *et al.* [1] showed that at energies near the Coulomb limit, the elastic scattering and direct reactions for collisions caused by the three Beryllium isotopes ^{9,10,11}Be on a medium weight target of ^{64}Zn were investigated. In the Coulomb-nuclear interference peak angular area, the elastic-scattering angular distribution of the ^{11}Be halo nucleus deviated from the classical Fresnel type diffraction operation. They estimated that overall reaction cross-sections for the ^{11}Be collision are more than a factor of two larger than those calculated for the collisions caused by ^{9,10,11}Be. They also discovered that transition and break-up mechanisms contribute significantly to the total reaction cross-section for ^{11}Be.

In 2013, S. Yusa *et al.* [41] showed that is in a random matrix model, they described excitations that were explicitly taken into account in their calculations of the coupled channels. The non-collective excitations will reproduce the calculated smearing of the peak structure in the ^{20}Ne+^{90}Zr barrier distribution while not greatly altering the structure in the ^{92}Zr system. In ^{90}Zr, the difference is mostly due to the closed neutron shell.

In 2014, E. C. Pinilla and P. Descouvemont [42] employed a microscopic continuum-discretized coupled-channels reaction framework (MCDCC) to study the elastic angular distribution of the ^{7}Li= α+t nucleus colliding with ^{12}C and ^{28}Si targets at E_{Lab}=350 MeV. In this framework, the ^{7}Li projectile is described in a microscopic cluster model and impinges on non-composite targets. The diagonal and coupling potentials are constructed from nucleon-target interactions and ^{7}Li microscopic wave functions. We obtain a fair description of the experimental

data, in the whole angular range studied, when continuum channels are included. The inelastic and breakup angular distributions on the lightest target are also investigated. In addition, we compute $^{7}Li+^{12}C$ MCDCC elastic cross sections at energies much higher than the Coulomb barrier and we use them as reference calculations to test the validity of multichannel eikonal cross sections.

In 2015, V. I. Kovalchuk [43] investigated cross-sections of total scattering of ^{6}He, ^{7}Be, and ^{8}B nuclei by ^{12}C nuclei and described in the context of the nuclear diffraction model and the nucleus-nucleus scattering model in the high-energy approximation with a double folding potential for the intermediate energies of the incident particles. The calculations took into account the Coulomb interaction and inelastic scattering with the excitation of the target's low-lying collective states and used measured nucleon density distributions.

In 2016, J. P. Fernández-García, *et al.* [44] used the continuum discrete coupling approach to test the experimental distributions of elastic scattering angular distributions of collisions that included the weakly bound nuclei $^{6,7}Li$ and the halo nucleus ^{6}He on the same ^{64}Zn target at several energies around the Coulomb barrier, while the $^{6}He+^{64}Zn$ was compared with all continuum discrete results.

In 2017, N. Burtebayev *et al.* [45] found optimal optical parameters to investigate the transfer mechanism at low energy, close to the Coulomb barrier energy for $^{15}N+^{16}O$ nuclear systems. The data were analyzed within the optical model (OM) and coupled reaction channels (CRC) method. The CRC calculation was used by the program code Fresco.

In 2018, S. R. Mokhtar *et al.* [46] investigated the $^{6}Li+^{40}Ca$ elastic scattering through the energy range 26–240 MeV in the framework of the optical model and α-cluster structure of the colliding nuclei. The double folding (DF) calculations for the real central part of the nuclear optical potential are performed

by folding the α-α and α-n effective interactions over the density distributions of α-clusters in the target (^{40}Ca) nucleus and considering the α-d structure of the projectile (^{6}Li) nucleus. The energy dependence of the corresponding reaction cross sections and real and imaginary volume integrals of the considered reaction are also investigated.

In 2019, Q. J. Tarbool, *et al.* [47] showed that large-angle total scattering at sub-barrier energies similar to the Coulomb barrier height for ^{6,7}Li + ^{64}Zn systems which is used to study the surface property of the inter-nucleus potential in heavy-ion reactions. Single-channel (SC) and coupled-channels (CC) calculations were performed.

In 2020, A. J. Hassan, and K. S. Jassim [48] investigated the effects of the surface diffuseness parameter on total scattering using the Woods-Saxon (WS) nuclear potential systems ^{6}He+^{64}Zn, ^{7}Li+^{64}Zn, and ^{8}Li+^{90}Zr.

In 2021, K. Wang *et al.* [49] studied elastic scattering and breakup angular distributions of the weakly bound radioactive nucleus ^{8}B on a ^{208}Pb target at an incident energy of 238 MeV, The data have been analyzed using the optical model and the continuum discretized coupled channels (CDCC) formalism. The measured and calculated elastic scattering angular distributions do not show any significant Coulomb rainbow suppression.

1.6 The aim of this research

The aim of thesis investigated the effect of coupling and breakup channels on systems involving stable and unstable nuclei projectile on medium and heavy mass targets as **^{6}He + ^{208}Pb**, **^{17}F + ^{208}Pb**, **^{7}Be + ^{58}Ni**, **^{7}Li + ^{59}Co**, **^{6}Li + ^{59}Co**, **^{16}O + ^{64}Zn**, **^{32}S+^{208}Pb**, and **^{11}Be+^{209}Bi**. To calculate the elastic and total scattering cross sections to Rutherford cross sections (σ_{el}/σ_R and σ_T/σ_R), and the distribution of the barrier (D_{el} or D_T) and compare the theoretical results with the corresponding experimental data.

Chapter Two

Theoretical Background

2.1 Introduction

A standard tool to analyze heavy-ion reactions at energies around the Coulomb barrier is the coupled-channels approach [50]. In addition to excitation properties of colliding nuclei, such as the excitation energy and deformation parameter, an inter-nucleus potential is one of the most important inputs for coupled-channels calculations. This is so, because nuclear reactions at sub barrier energies are primarily governed by the height, the position, and the curvature of the Coulomb barrier. Also, the coupling form factors are generated from the inter-nucleus potential. In addition, the coupling form factors are created from the inter-nucleus potential. Numerous methods are suggested to calculate the real part of the inter-nuclear potential. Among them, the double folding model has been often used and has enjoyed a success in describing elastic and inelastic scattering for many systems [51]. The Woods-Saxon form, which conforms to the double folding potential of the tail region, has also often been used to parameterize the inter-nuclear potential [52]. Many experimental evidence has emerged, in recent years, presenting that double folding potential did not actually account for the fusion of energy cross-sections near the Coulomb barrier [53].

2.2 The nuclear system potential

Due to the electrostatic repulsion present between the positively charged target nucleus and the positively charged projectile there is difficulty in the penetration of the much familiar barrier known as the Coulomb barrier. The system is straightforwardly described in terms of their relative motion in the center-of-mass system, as the two associates are of comparable mass. Assuming the standard laboratory situation of a fixed target, which is bombarded with a beam of projectile nuclei, the relation between the kinetic energy E_{lab} as measured in the laboratory system and the kinetic energy E_{cm} in the center-of-mass system is given by [54],

$$E_{cm} = \frac{A_T}{A_T + A_P} E_{lab} \tag{2.1}$$

where A_P and A_T represent the mass number of the projectile and target nuclei, respectively. Electron mass and differences in binding energy per nucleon may be ignored as a good approximation. The motion of the center-of-mass is fully determined by the kinematics of the reaction and can be calculated from the bombarding energy and the nuclear masses. Quantum mechanically the nuclear binary system may be represented by the wave function $\Psi(\vec{r})$. Using the center-of-mass parameterization, the combined effect of the Coulomb and the nuclear force between the two nuclei can be expressed as the interaction potential. These have been illustrated in Fig. 2.1 [54],

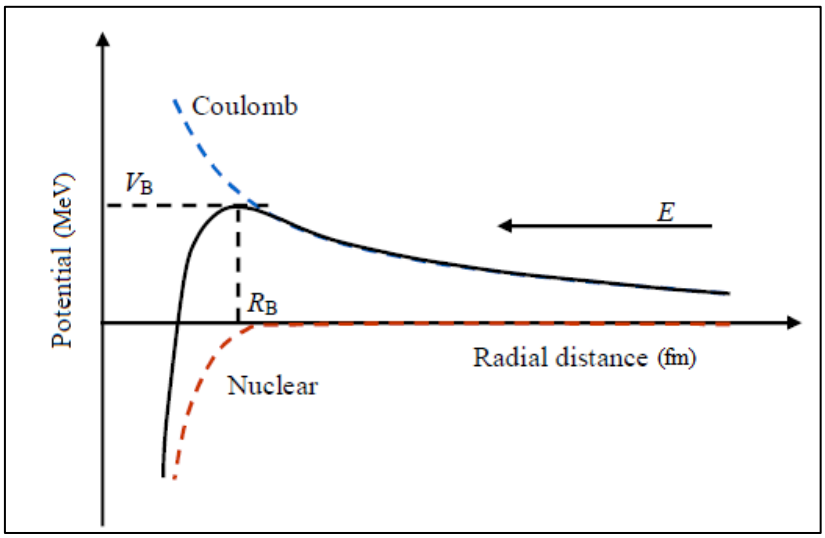

Figure 2.1 : The illustration of the forces that form a Coulomb barrier between the participating nuclei in a nuclear reaction [54].

$$V(r) = V_C(r) + V_N(r) \tag{2.2}$$

where V_C is the Coulomb and V_N is the nuclear potential. The motion of the binary system is then described by the Schrödinger equation [55],

$$\left[-\frac{\hbar^2}{2\mu}\frac{d^2}{dr^2} + \frac{\ell(\ell+1)\hbar^2}{2\mu r^2} + V(r) - E\right]\Psi(\vec{r}) = 0 \tag{2.3}$$

At large distances r, the Coulomb potential $V_C(r)$ has the form of the electrostatic potential for two point-charges. At close approach, when the charge distributions overlap, the point-charge has to be modified. This is often achieved by replacing one of the point charges with a homogeneously charged sphere of radius R_C , so that [56],

$$V_C(r) = \begin{cases} \dfrac{Z_P Z_T e^2}{r} & \text{for } r > R_C \\ \dfrac{Z_P Z_T e^2}{R_C}\left(\dfrac{3}{2} - \dfrac{1}{2}\dfrac{r^2}{R_C^2}\right) & \text{for } r \leq R_C \end{cases} \tag{2.4}$$

since during the collision, there occur, a large number of interactions between the projectile and the target nucleons, It has not been possible to determine the nuclear potential $V_N(r)$ from the known two-body forces between nucleons. It is, therefore, common practice to make a simple parameterization, approximating the nuclear potential with a function which resembles the nuclear mass distribution. This results in the Woods-Saxon potential [57],

$$V_N(r) = \frac{-V_0}{1 + \exp\left[\dfrac{r - R_0}{a_0}\right]} \tag{2.5}$$

where V_0 refers to the potential depth and a_0 is the diffuseness of the potential. The radius R_0 of the nuclear potential is given by [57],

$$R_0 = r_0\left[A_P^{1/3} + A_T^{1/3}\right] \tag{2.6}$$

where r_0 is the radius parameter. It is worthwhile to mention that the potential parameters V_0, a_0 and r_0 are not unique. Hence, they are usually adjusted by fitting experimental data.

2.3 Single channel description

The detailed behavior of cross sections in heavy-ion reactions depends strongly on the intrinsic degrees of freedom of the nuclei involved. However, according to the optical model [58,59], the gross features of the elastic and the total reaction cross sections can be described by a simple Schrödinger equation in the space of the projectile–target separation degree of freedom. In this model, the channel-coupling effects on the elastic channel are represented by the complex energy-dependent potential [58],

$$U^{opt}(r) = V^{opt}(r) - iW^{opt}(r) \tag{2.7}$$

The real part of the interaction, $V^{opt}(r)$, can be written in the form [58],

$$V^{opt}(r) = V_N(r) + V_C(r) \tag{2.8}$$

Where $V_C(r)$ is a long-range term corresponding to the Coulomb forces between the collision partners and $V_N(r)$ is a short range term associated with the nuclear forces. The imaginary part, $W^{opt}(r)$, is a short-range function accounting for the incident flux lost to excited channels. In this way, the reaction dynamics is governed by the Schrödinger equation [59],

$$[T + V^{opt}(r) - iW^{opt}(r)]\psi^{(+)}(\vec{r}) = E\,\psi^{(+)}(\vec{r}) \tag{2.9}$$

where T is the kinetic energy for the projectile–target relative motion and E is its total energy. The wave function can be written as [59],

$$\psi^{(+)}(\vec{r}) = \phi_C(\vec{r},\vec{k}) + \psi^{sc}(\vec{r},\vec{k}) \tag{2.10}$$

where $\vec{k}$ is the incident wave vector, $\phi_C(\vec{r},\vec{k})$ is the wave function for pure Coulomb scattering (that is, setting $V_N(r) = W^{opt}(r) = 0$) and $\psi^{sc}(\vec{r},\vec{k})$ is the correction of the scattered wave arising from $V_N(r)$ and $W^{opt}(r)$. These wave functions satisfy the scattering boundary conditions [60],

$$\phi_C(\vec{r},\vec{k})_{r\to\infty} \longrightarrow \frac{1}{\sqrt{8\pi^3}}\left[e^{i(kz-\eta_s \ln(kr-kz))} + f_C(\theta)\frac{e^{i(kz-\eta_s \ln 2kr)}}{r}\right] \tag{2.11}$$

$$\psi^{sc}(\vec{r},\vec{k})_{r\to\infty} \to \frac{1}{\sqrt{8\pi^3}}\left[f_N(\theta,\phi)\frac{e^{i(kz-\eta_s \ln 2kr)}}{r}\right] \tag{2.12}$$

above, $f_C(\theta)$ is the Coulomb scattering amplitude, which is known analytically, and $f_N(\theta,\phi)$ is the scattering amplitude associated with the short-range interaction. The latter is usually expanded in partial-waves and calculated numerically. The elastic scattering cross sections is given by the scattering amplitudes through the expression, respectively [61],

$$\frac{d\sigma_{el}(E,\theta)}{d\Omega} = |f_C(\theta) + f_N(\theta,\phi)|^2 \tag{2.13}$$

2.4 Continuum discretized coupled channel (CDCC) formalism

Consider the reaction described by the total wave function $\Psi(\vec{r},\tau)$, where $\vec{r}$ stands for the projectile and target nuclei separation vector and τ for the set of intrinsic coordinates of the projectile and target nuclei. The dynamics of this reaction is determined by the Hamiltonian,

$$H = H_0 + T + U \tag{2.14}$$

where $H_0 \equiv H_0(\tau, p_\tau)$ is the intrinsic Hamiltonian, $T \equiv -\hbar^2\nabla^2/2\mu$ is the kinetic energy operator of the relative motion between the projectile and target nuclei, and $U \equiv U(\vec{r},\tau)$ is the interaction potential. The eigenstates of the intrinsic Hamiltonian, $|\eta\rangle$, satisfy the Schrödinger equation [62],

$$\left(e_\eta - H_0\right)|\eta\rangle \quad = 0 \tag{2.15}$$

The orthonormality is,

$$\langle\eta'|\eta\rangle = \int d\tau\, \varphi^*_{\eta'}(\tau)\, \varphi_\eta(\tau) = \delta_{\eta\eta'} \tag{2.16}$$

where $\varphi_\eta\,(\tau)$ $\left(\varphi_{\eta'}\,(\tau)\right)^*$ is the wave function corresponding to the state $|\eta\rangle$ ($|\eta\rangle)^*$ in the τ- representation. The interaction potential is split as,

$$U = U' + U'' \tag{2.17}$$

Where U' is diagonal in channel space,

$$U' = \sum_{\eta} |\eta\rangle\, U'_{\eta}\, \langle\eta| \tag{2.18}$$

$$U'' = \sum_{\eta} |\eta\rangle\, U''_{\eta,\eta'}\, \langle\eta'| \tag{2.19}$$

Where

$$U'_{\eta}(\vec{r}) = \int d\tau \left|\varphi_{\eta}(\tau)\right|^2 U'(\vec{r},\tau) \tag{2.20}$$

$$U''_{\eta,\eta'}(\vec{r}) = \int d\tau\, \varphi^*_{\eta'}(\tau)\, U''(\vec{r},\tau)\, \varphi_{\eta}(\tau) \tag{2.21}$$

The potential U' is arbitrary, except for the condition of being diagonal in channel space. However, once it is chosen, U'' is given by the relation $U'' = U - U'$. Frequently, it is convenient to choose U' such that U'' is purely off diagonal. In such cases the components of U'' can be written [62],

$$U''_{\eta,\eta'}(\vec{r}) = \int d\tau\, \varphi^*_{\eta'}(\tau)\, U''(\vec{r},\tau)\, \varphi_{\eta}(\tau) - \delta_{\eta\eta'}\, U'_{\eta}(\vec{r}) \tag{2.22}$$

From the Schrödinger equation, we can start to derive the coupled channel equations,

$$(E - H)\left|\Psi_{\eta}\left(\eta_0, \vec{k}_0\right)\right\rangle = 0 \tag{2.23}$$

and the channel-expansion,

$$\left|\Psi_{\eta}\left(\eta_0, \vec{k}_0\right)\right\rangle = \sum_{\eta}\left|\psi_{\eta}\left(\eta_0, \vec{k}_0\right)\right\rangle |\eta\rangle \tag{2.24}$$

The notation $\left|\Psi\left(\eta_0, \vec{k}_0\right)\right\rangle$ indicates that the collision is started in channel η_0, with wave vector $\vec{k}_0$, and the energy scale is chosen such that $e_{\eta_0} = 0$. The Schrödinger equation solution has components $\left|\Psi_{\eta}\left(\eta_0, \vec{k}_0\right)\right\rangle$ for both $\eta = \eta_0$ and $\eta \neq \eta_0$, The infinite expansion of Eq. (2.24) is truncated so as to include only the

most relevant channels or closed coupling approximation. To account for the loss of flux through neglected channels, One may include an imaginary part in the channel potentials $U'_{\eta}(\vec{r})$. To find the wave function, we must write the Hamiltonian as [62].

$$H = H_0 + H' + U'' \tag{2.25}$$

where

$$H' = T + U' \tag{2.26}$$

When we put Eqs. (2.24) and (2.25) into Eq. (2.23), and take the scalar product with each intrinsic state $\langle\eta|$, then we get the coupled channel equations,

$$\left(E_\eta - H'_\eta\right)\left|\psi_\eta\left(\eta_0, \vec{k}_0\right)\right\rangle = \sum_{\eta'} U''_{\eta,\eta'}(\vec{r})\ \left|\psi_{\eta'}\left(\eta_0, \vec{k}_0\right)\right\rangle \tag{2.27}$$

or,

$$\left[E_\eta + \frac{\hbar^2}{2\mu}\nabla^2 - U'_\eta(\vec{r})\right]\psi_\eta(\vec{r}) = \sum_{\eta'} U''_{\eta,\eta'}(\vec{r})\ \psi_{\eta'}(\vec{r}) \tag{2.28}$$

These equations are usually solved using incoming wave boundary conditions [63].

$$\psi_\eta(\vec{r}) \to T_\eta\ exp\left(-i \int_{r_{abs}}^{r} k'_\eta\left(r'\right) dr'\right), \qquad r \le r_{abs} \tag{2.29}$$

$$\psi_\eta(\vec{r}) \to \frac{i}{2} H_l^{(-)}\left(k_\eta r\right) + \sqrt{\frac{k}{k_\eta}}\, S_\ell\ H_l^{(+)}\left(k_\eta r\right), \qquad r > r_{abs} \tag{2.30}$$

Where the potential pocket at $r = r_{abc}$ is minimal, $k_\eta = \sqrt{\frac{2\mu E_\eta}{\hbar^2}}$ and $k = \sqrt{\frac{2\mu E}{\hbar^2}}$ and the local wave number $k'_\eta(r)$ is [64] .

$$k'_\eta(r) = \sqrt{\frac{2\mu}{\hbar^2}\ \left(E_\eta\ - V_{eff}(r) - U'_\eta(\vec{r})\ \right)} \tag{2.31}$$

If we have the transmission coefficients, we can proceed with the rest of the process T_η. The amplitude of scattering $f_T(E, \theta)$ is given by [65],

$$f_T^{(\eta)}(E,\theta) = f_C(E,\theta) + f_N^{(\eta)}(E,\theta) \tag{2.32}$$

Were $f_C(E,\theta)$ is Coulomb amplitude of scattering, $f_N^{(\eta)}(E,\theta)$ nuclear amplitude of scattering. The scattering differential cross section is evaluated as [66].

$$\frac{d\sigma_{el}}{d\Omega}(E,\theta) = \frac{k_{\eta_0}}{k}\left|f_T^{(\eta_0)}(E,\theta)\right|^2 = \frac{k_{\eta_0}}{k}\left|f_C(E,\theta) + f_N^{(\eta_0)}(E,\theta)\right|^2 \tag{2.33}$$

$$\frac{d\sigma_{in}}{d\Omega}(E,\theta) = \sum_{\eta\neq\eta_0}\frac{k_\eta}{k}\left|f_N^{(\eta)}(E,\theta)\right|^2 \tag{2.34}$$

$$\frac{d\sigma_T}{d\Omega}(E,\theta) = \sum_{\eta}\frac{k_\eta}{k}\left|f_T^{(\eta)}(E,\theta)\right|^2 \tag{2.35}$$

Rutherford cross section evaluated by [67].

$$\frac{d\sigma_R}{d\Omega}(E,\theta) = |f_C(E,\theta)|^2 \tag{2.36}$$

2.5 Approximate formulation of scattering cross section

We now need to figure out how to define a similar test function for a scattering problem. In the limit of a strong Coulomb field, the cross sections for elastic scattering at $\theta = \pi$ are given by the pure classical approach,

$$\sigma_{el}^{cl}(E,\pi) = \sigma_R(E,\pi)\,\theta(V_b - E) \tag{2.37}$$

where $\sigma_R(E,\pi)$ is known as the Rutherford cross section. The scattering barrier distribution is given by [68].

$$D_T(E) = -\frac{d}{dE}\left(\frac{\sigma_T(E,\pi)}{\sigma_R(E,\pi)}\right) \tag{2.38}$$

In realistic systems, however, the cross section of total scattering deviates from the Rutherford cross section even at energies below the barrier due to the effect of nuclear distortion. Using semi-classical theory [69-71], semi-classical

formula was derived a for backward scattering that takes the nuclear effect to the leading order into account. The result for a scattering angle $\theta = \pi$ is as follows:

$$\sigma_{el}(E,\pi) = \sigma_R(E,\pi)\alpha(E,\lambda_C).|S(E,\lambda_C)|^2 \quad (2.39)$$

where $S(E,\lambda_C)$ denotes the total (Coulomb + nuclear) S-matrix at energy E and angular momentum $\lambda_C = \eta_S\, cot(\theta/2)$, and η_S is the standard Sommerfeld parameter. It is worth noting that $|S(E,\lambda_C)|^2$ is nothing more than the reflection probability of the Coulomb barrier. For $\theta = \pi$, λ_C equals zero, $|S(E,\lambda_C = 0)|^2$ is given by

$$|S(E,\lambda_C = 0)|^2 = R(E) = \frac{exp\left[-\frac{2\pi}{\hbar\Omega}(E - V_b)\right]}{1 + exp\left[-\frac{2\pi}{\hbar\Omega}(E - V_b)\right]} \quad (2.40)$$

in terms of the parabolic approximation. $\alpha(E,\lambda c)$ in Eq. (2.39) is given by

$$\alpha(E,\lambda_C) = 1 + \frac{V_N(r_c)}{ka}\frac{\sqrt{2a_0\pi k\eta_S}}{E}\left[1 - \frac{r_c}{Z_P Z_T e^2}.2V_N(r_c)\left(\frac{r_c}{a_0} - 1\right)\right] \quad (2.41)$$

where $k = \sqrt{2\mu E/\hbar^2}$), and μ is the reduce mass of the colliding system. Nuclear potential $V_N(r_c)$ is assessed at the Coulomb's turning point $r_c = \left(\eta_S + \sqrt{\eta_S^2 + \lambda_c^2}\right)/k$, and a_0 is the nuclear potential's diffuseness parameter.

2.6 Scattering barrier distribution

The sum scattering from the contribution of inelastic and elastic reactions, as well as all other processes from direct reactions including transition and breakup, is known as complete scattering. The probability of transmission through the angular momentum barrier is related to fusion $\ell = 0$, $T_0(E)$, and the large-angle total scattering is related to the probability of reflection, $R_0(E)$. Due to the retention of the reaction flux, $T_0(E) + R_0(E) = 1$, the backscattering of

total scattering may be considered to be complementary to the fusion. The total scattering barrier distribution $D_T(E)$ is defined as [72].

$$D_T(E) = -\frac{d}{dE}\left[\frac{\sigma_T}{\sigma_R}(E)\right] \tag{2.42}$$

where σ_T/σ_R is the ratio of total scattering cross sections to Rutherford cross sections. These approaches have the advantage of requiring a numerical assessment of first derivatives rather than second derivatives, as in mergers. In addition, in most cases, the measurement of total and elastic scattering is easier than cross-section fusion.

Chapter Three

Results, Discussion and Conclusions

3.1 Introduction

The effect of the break-up of weakly bound structures on different reaction and dispersion mechanisms has been extensively investigated, where the experimental angular distributions for elastic scattering were proposed for close-barrier energy and optical potential energy dependence [73]. The (CDCC) calculations have shown that the suppression of the peaks of the Coulomb nuclear intrusion [74].

The experimental angular distributions were analyzed by means of (CDCC) approach, in addition to the elastic dispersion angular distributions described [75]. Abnormal elastic dispersion cross-section. Coupling with non-elastic structures affects elastic scattering.

In particular, in the case of tightly bound nuclei, the elastic dispersion cross-sections are exhausted when coupling with dispersion channels is required. Other primary signatures in halo nucleus reactions with solid targets include the departure of the elastic cross-section from the Rutherford cross-section at sub-Coulomb energies and the depletion of the Fresnel peak at near-barrier energies [76].

3.2 Results and Discussion

In this thesis consider that the nuclear potential has a Akyüz-Winther potential for **^{6}He + ^{208}Pb**, **^{17}F + ^{208}Pb**, **^{7}Be + ^{58}Ni**, **^{7}Li + ^{59}Co**, **^{6}Li + ^{59}Co**, **^{16}O + ^{64}Zn**, **^{32}S+^{208}Pb**, and **^{11}Be+^{209}Bi**, to calculate the elastic and total scattering cross sections to Rutherford cross sections ($d\sigma_{el}/d\sigma_R$ and $d\sigma_T/d\sigma_R$), and the distribution of the barrier (D_{el} or D_T).

The CDCC method have been employed no coupled and coupled-channels (CC) calculations by program which called CC_SCT code. The scattering barrier distribution D_{el} or D_T has been calculated by using the numerical two-point-difference method by sub-program, also this method using to extract experimental

data of the scattering barrier distribution. The parameters used in the calculations of cross section were extracted from the optical potential fits, to achieve the optimum comparability between the theoretical estimates of cross sections and empirical values for the systems reviewed. The Woods-Saxon parameters of Akyüz-Winther potential are listed in Table 3.1.

Table 3.1: Akyüz-Winther potential parameters, energy and scattering angle center of mass for some Selected Systems nuclear reactions.

System	V_0 (MeV)	r_0 (fm)	a_0 (fm)	W_0 (MeV)	r_i (fm)	a_i (fm)	V_b (MeV)	$E_{c.m.}$ (MeV)	$\theta_{c.m.}$ (deg)
$^{6}He+^{208}Pb$	80.0	1.2	0.63	46.7	1.35	0.78	26.0	21.38	61
$^{17}F+^{208}Pb$	20.3	1.2	0.63	181.4	1.16	0.67	---	87.36	---
$^{7}Be+^{58}Ni$	50.6	1.2	0.63	16.9	1.35	0.62	16.02	17.78	128
$^{7}Li+^{59}Co$	51.4	1.2	0.63	17.1	1.35	0.48	13.8	10.27	84
$^{6}Li+^{59}Co$	48.9	1.2	0.63	16.3	1.35	0.46	14.2	10.89	83
$^{16}O+^{64}Zn$	62.0	1.2	0.63	20.7	1.25	0.65	46.9	38.4	61
$^{11}Be+^{209}Bi$	90.2	1.2	0.63	130.1	1.29	0.77	---	38.0	---
$^{32}S+^{208}Pb$	205.2	1.1	0.63	68.4	1.34	0.56	146.0	---	105

3.2.1 ^{6}He+^{208}Pb reaction

In the ^{6}He+^{208}Pb system, the results of this reaction are taken the elastic cross section to the Rutherford cross section σ_{el}/σ_{R} was determined with angle center of mass θ_{cm} (in figure 3.1, panel A), energy center of mass E_{cm} (in figure 3.1, panel B). The elastic scattering barrier distribution D_{el} was calculated with energy center of mass E_{cm} (in figure 3.1, panel C). The calculations have been performed for all order coupling channels in the nuclear system ^{6}He+^{208}Pb, where the projectile ^{6}He is two neutron halo nucleus and the target ^{208}Pb is heavy ion, with Akyüz-Winther potential parameters $V_0 = 80.0\ MeV$, $a_0 = 0.63\ fm$, $r_0 = 1.2\ fm$, $W_0 = 46.7\ MeV$, $a_i = 0.78\ fm$, and $r_i = 1.35\ fm$ which are listed in Table 3.1.

In figure 3.1 panel (A) a good agreement in limits of angle from 20° – 65° with experimental data in coupling states but with more closeness to the experimental data within the angle limits from 125° – 170° in the case of no coupling.

In panel (B) and (C) a good agreement between theoretical calculations and experimental data in down region Coulomb barrier in coupled and uncoupled calculations.

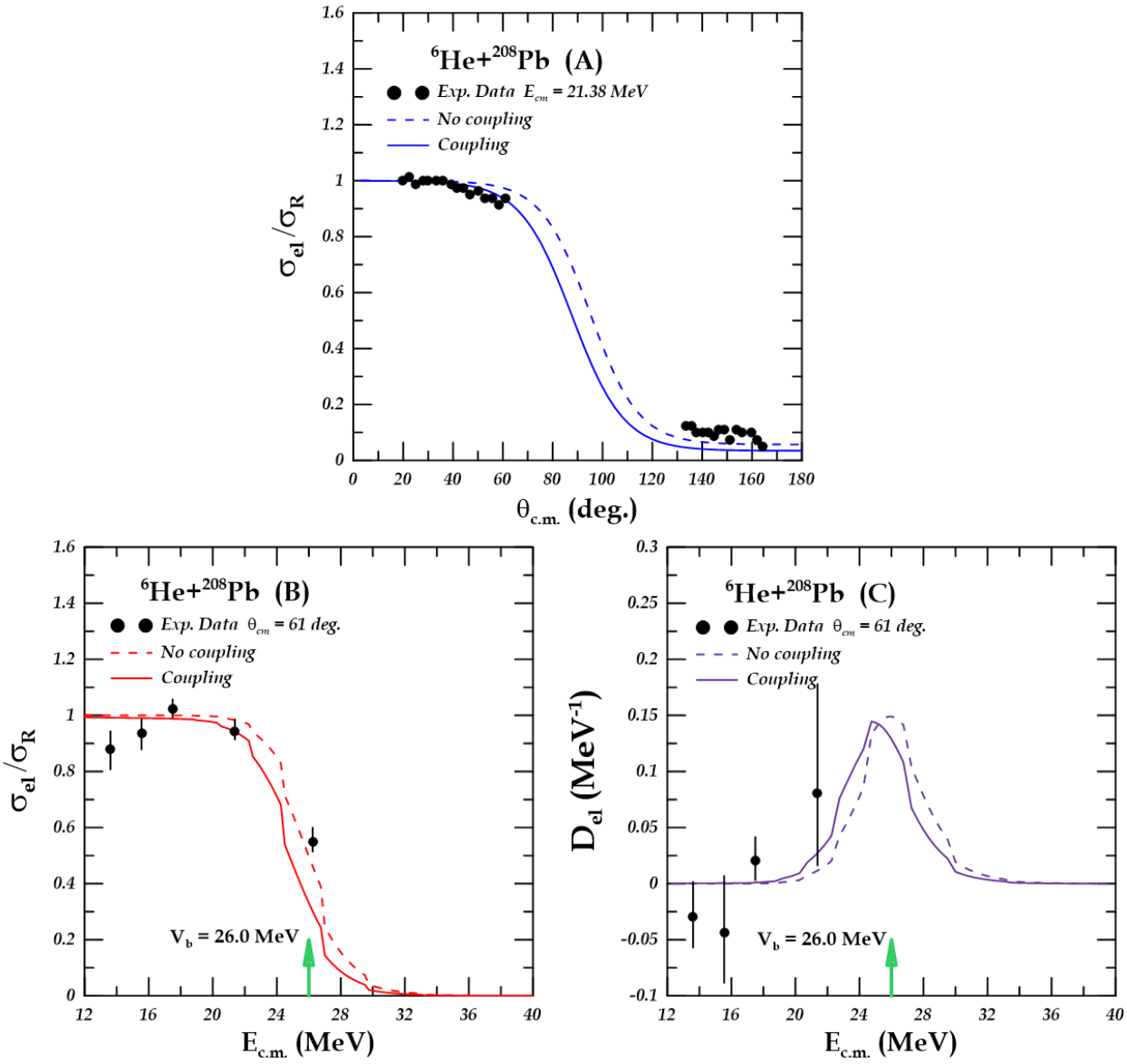

Figure 3.1 : Uncoupled channel and coupled channels calculations for ^{6}He+^{208}Pb system by dashed and solid curves respectively: **(A)** elastic scattering cross section with the mass center angle, **(B)** elastic scattering cross section with energy center of mass, **(C)** elastic scattering barrier distribution with the energy center of mass, the black circles are experimental data from Ref. [77].

3.2.2 ^{17}F+^{208}Pb reaction

In the ^{17}F+^{208}Pb system, the results of this reaction are taken the total cross section to the Rutherford cross section σ_{el}/σ_R was determined with angle center of mass θ_{cm} (in figure 3.2).

The calculations have been performed for the nuclear system ^{17}F+^{208}Pb where the projectile ^{17}F is one proton halo nucleus and the target ^{208}Pb is heavy ion. The Akyüz-Winther potential parameters $V_0 = 20.3\ MeV$, $a_0 = 0.63\ fm$, $r_0 = 1.2\ fm$, $W_0 = 181.4\ MeV$, $a_i = 0.67\ fm$, and $r_i = 1.16\ fm$, which are listed in Table 3.1. A acceptable match between theoretical calculations and experimental data in coupled and uncoupled calculations.

And the dispersion of experimental values because the ^{17}F nucleus is one proton halo, and the disintegration occurs due to the coupling of the breakup channel which causes the dispersion of the experimental data at multiple angles.

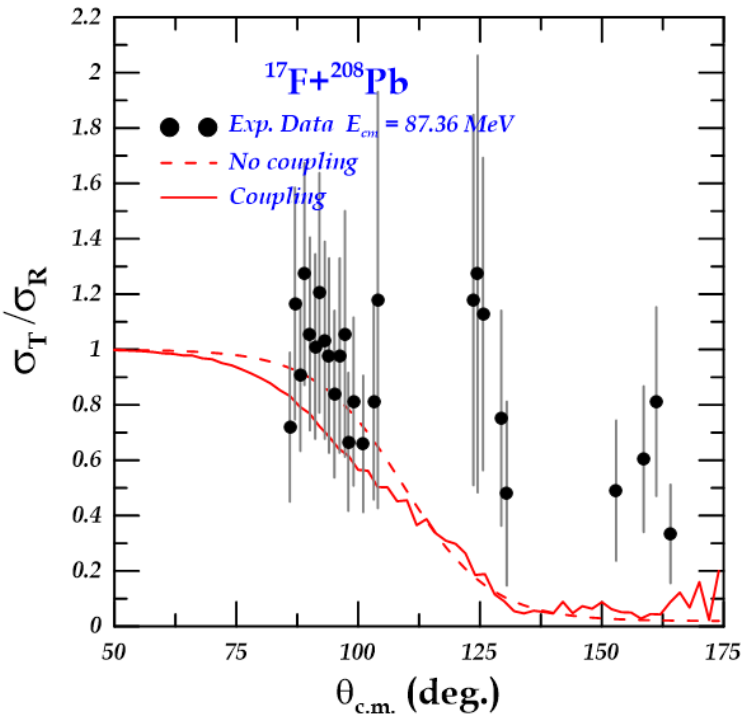

Figure 3.2 : Uncoupled channel and coupled channels calculations for ^{17}F+^{208}Pb system by red dashed and solid curves of total scattering cross section with the mass center angle, the black circles are experimental data from Ref. [78].

3.2.3 ^{7}Be+^{58}Ni reaction

In the ^{7}Be+^{58}Ni system, (see figure 3.3) the results of this reaction are taken the elastic cross section to the Rutherford cross section was determined with angle center of mass θ_{cm} (A), energy center of mass E_{cm} (B).

The elastic scattering barrier distribution D_{el} was calculated with energy center of mass E_{cm} (in figure 3.3, C). The calculations have been performed for the nuclear system ^{7}Be+^{58}Ni where the projectile ^{7}Be is weakly bound nucleus and the target ^{58}Ni is medium mass nucleus.

The Akyüz-Winther potential parameters $V_0 = 50.6\ MeV$, $a_0 = 0.63\ fm$, $r_0 = 1.2\ fm$, $W_0 = 16.9\ MeV$, $a_i = 0.62\ fm$, and $r_i = 1.35\ fm$. Excellent compatibility between theoretical calculations and experimental data above and down Coulomb barrier, indicated by green arrow on the $E_{m.c.}$ axis, in coupled and uncoupled calculations.

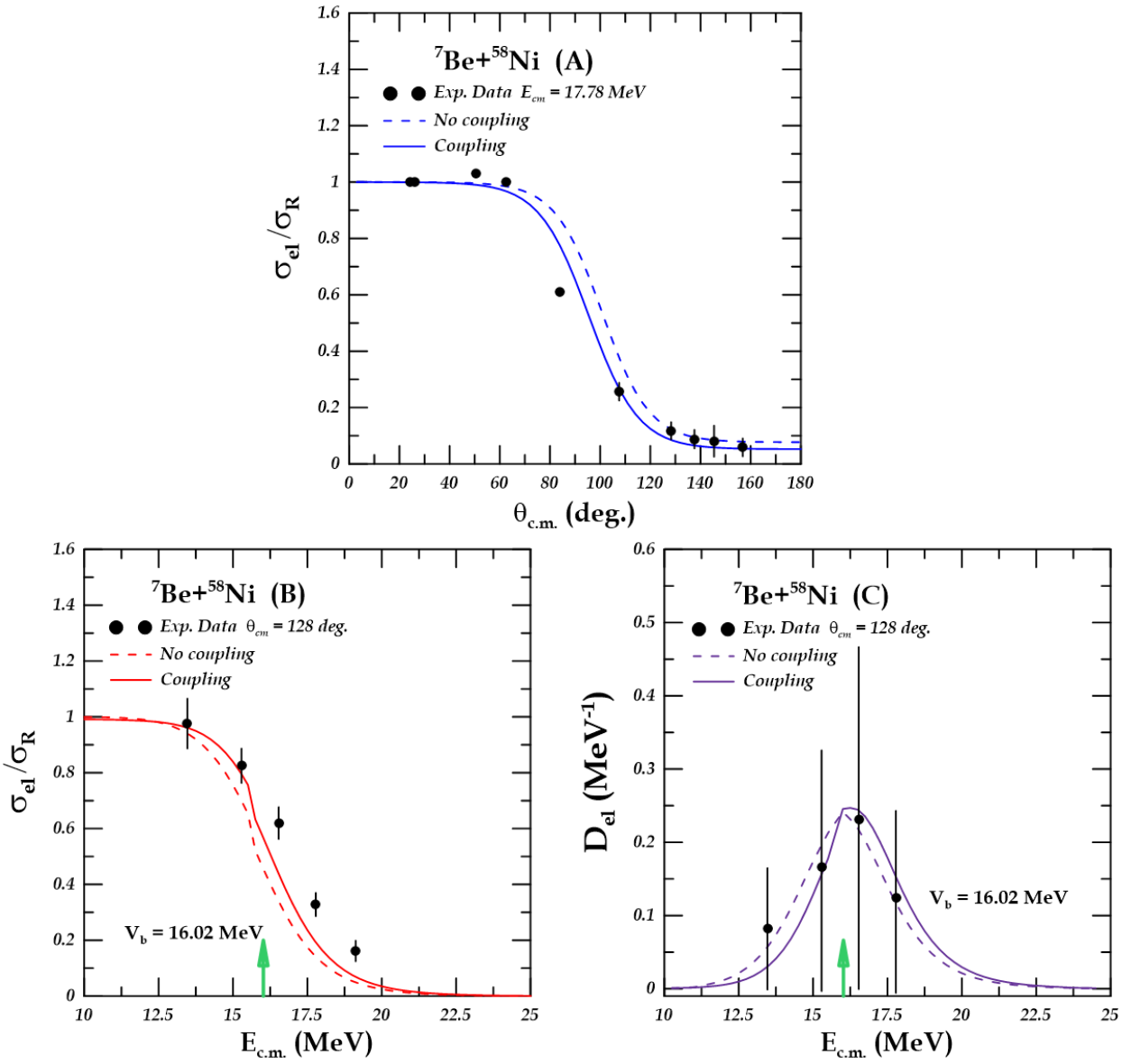

Figure 3.3 : Uncoupled channel and coupled channels calculations for $^{7}Be+^{58}Ni$ system by dashed and solid curves respectively: **(A)** elastic scattering cross section with mass center angle, **(B)** elastic scattering cross section with energy center of mass, **(C)** elastic scattering barrier distribution with the energy center of mass, the black circles are experimental data from Ref. [79].

3.2.4 ^{7}Li+^{59}Co reaction

In the ^{7}Li+^{59}Co system, the results of this reaction are taken the elastic cross section to the Rutherford cross section σ_{el}/σ_{R} was determined with angle center of mass θ_{cm} (in figure 3.4, A), energy center of mass E_{cm} (in figure 3.4, B).

The elastic scattering barrier distribution D_{el} was calculated with energy center of mass E_{cm} (in figure 3.4, C). The projectile ^{7}Li is weakly bound nucleus and the target ^{59}Co is medium mass nucleus, the Akyüz-Winther potential parameters $V_0 = 51.4\ MeV$, $a_0 = 0.63\ fm$, and $r_0 = 1.2\ fm$, , $W_0 = 17.1\ MeV$, $a_i = 0.48\ fm$, and $r_i = 1.35\ fm$**,** which are listed in Table 3.1.

In panel (A) the calculations of the cross section as function of angle θ_{cm} in perfect match with experimental data in coupled state. As such the cross section as function of energy E_{cm} in panel (B), excellent agreement for both coupled and no coupled cases with data above and under barrier and the elastic scattering barrier distribution in more closeness for no coupled channel with measured values around Coulomb barrier.

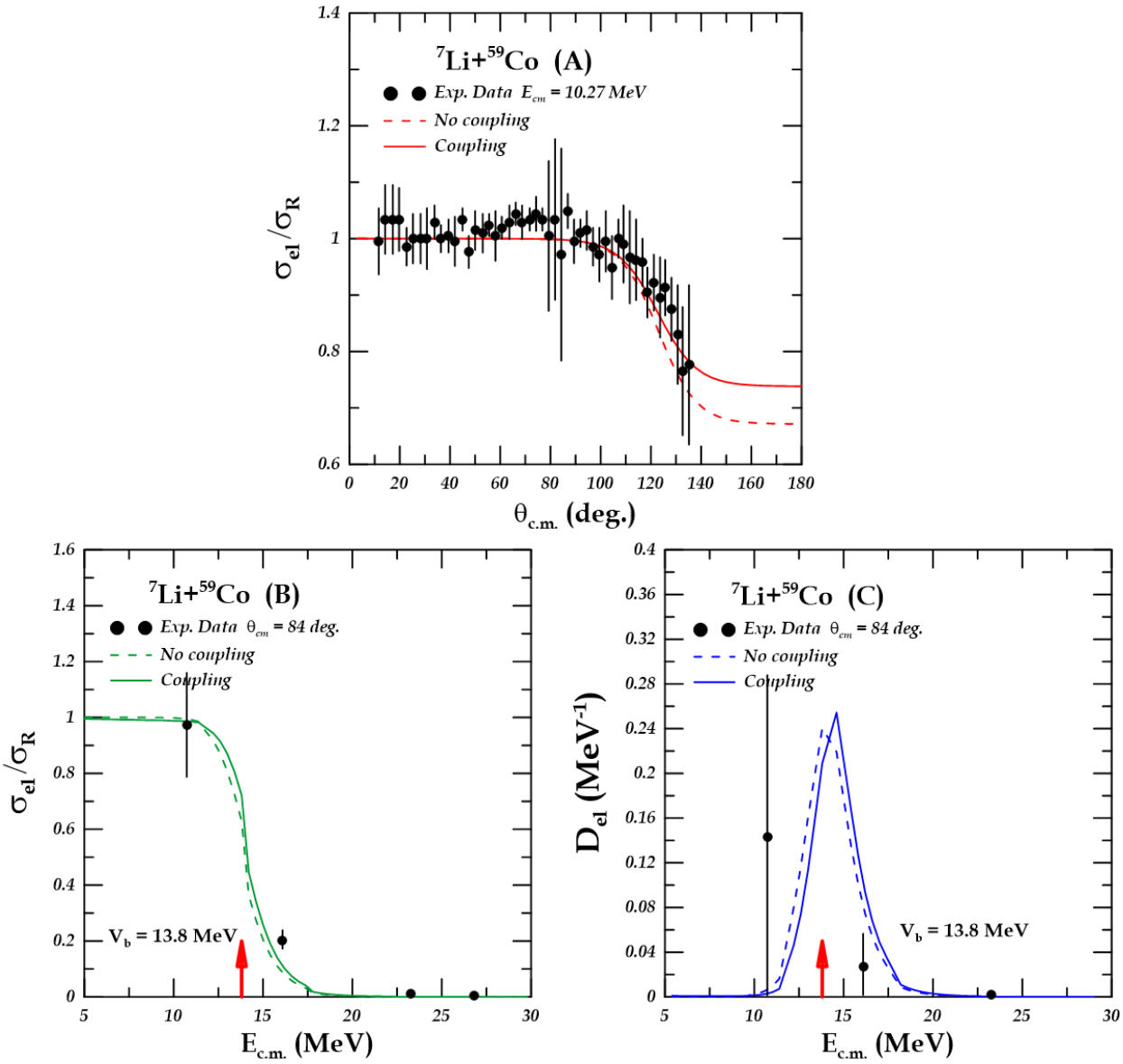

Figure 3.4 : Uncoupled channel and coupled channels calculations for ^{7}Li+^{59}Co system by dashed and solid curves respectively: **(A)** elastic scattering cross section with the mass center angle, **(B)** elastic scattering energy center of mass cross section, **(C)** elastic scattering barrier distribution with the energy center of mass, the black circles are experimental data from Ref. [80].

3.2.5 ^{6}Li+^{59}Co reaction

In the ^{6}Li+^{59}Co system, (see figure 3.5) the results of this reaction are taken the elastic cross section to the Rutherford cross section are determined with angle center of mass θ_{cm} (A), and energy center of mass E_{cm} (B), the black circles act experimental data from Ref. [80].

The elastic scattering barrier distribution D_{el} was calculated with energy center of mass E_{cm} (in figure 3.5, C).

The calculations have been performed for the nuclear system ^{6}Li+^{59}Co where the projectile ^{6}Li is stable nucleus and the target ^{59}Co is medium mass nucleus, the Akyüz-Winther potential parameters $V_0 = 48.9\,MeV$, $a_0 = 0.63\,fm$, and $r_0 = 1.2\,fm$, $W_0 = 16.3\,MeV$, $a_i = 0.46\,fm$, and $r_i = 1.35\,fm$, which are listed in Table 3.1.

Perfect agreement between cross section to the Rutherford cross section with angle center of mass calculations and experimental data in penal (A) of coupled channel. Around Coulomb barrier measured values converge well to coupled and uncoupled calculations of elastic cross section to the Rutherford cross section with energy center of mass. But elastic scattering barrier distribution results with energy center of mass get closer to data in uncoupled channel.

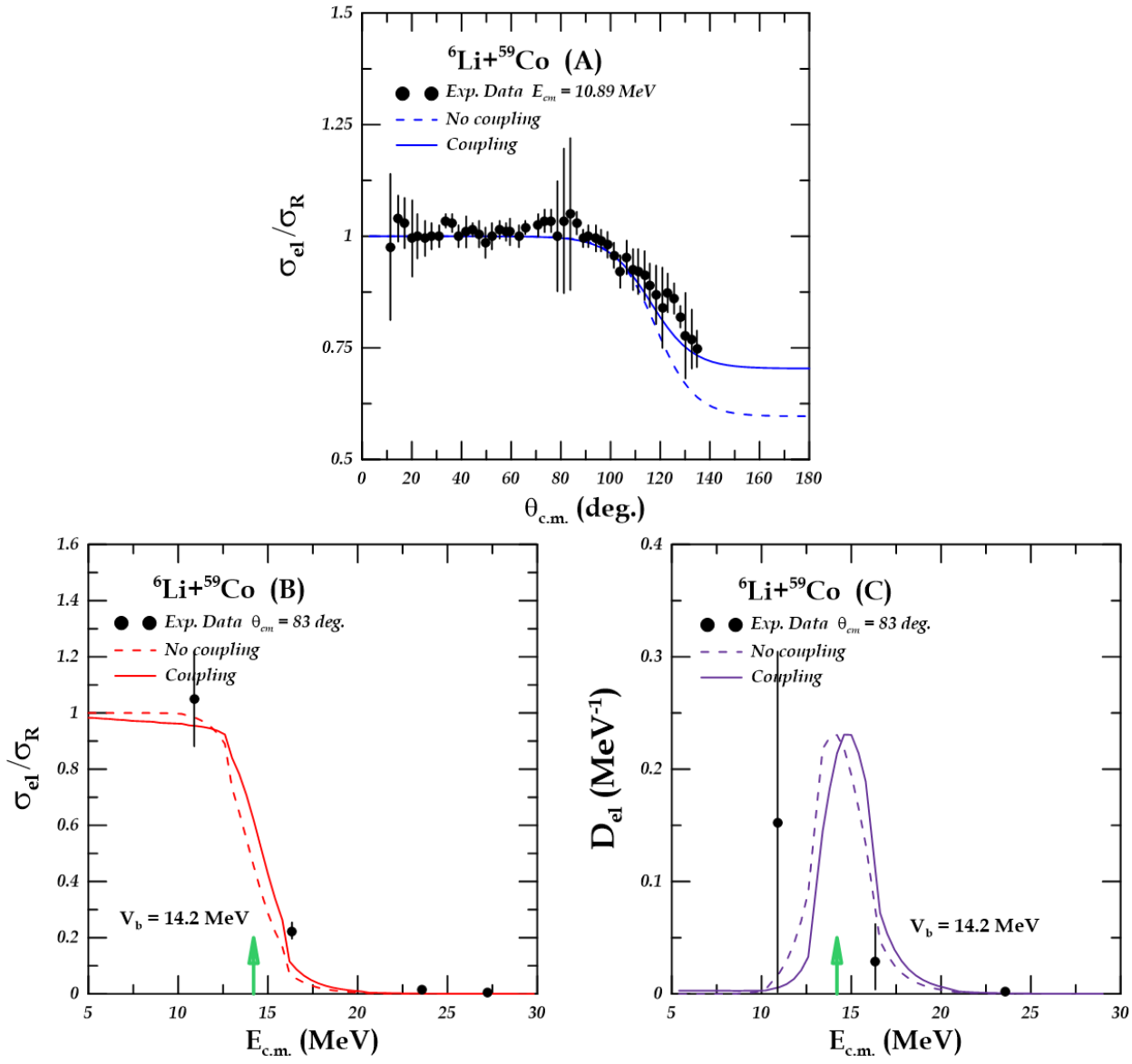

Figure 3.5: Uncoupled channel and coupled channels calculations for ^{6}Li+^{59}Co system by dashed and solid curves respectively: **(A)** elastic scattering cross section with the mass center angle, **(B)** elastic scattering cross section with energy center of mass, **(C)** elastic scattering barrier distribution with energy center of mass, the black circles are experimental data from Ref. [81].

3.2.6 $^{16}O+^{64}Zn$ reaction

In figure 3.6, the results of $^{16}O+^{64}Zn$ reaction are taken the elastic cross section to the Rutherford cross section was determined with angle center of mass θ_{cm} (panel A), energy center of mass E_{cm} (panel B).

The elastic scattering barrier distribution D_{el} was calculated with energy center of mass E_{cm} (in figure 3.6, panel C). The calculations have been performed for the nuclear system $^{16}O+^{64}Zn$ where the projectile ^{16}O is stable nucleus and the target ^{64}Zn is medium mass nucleus, the Akyüz-Winther potential parameters $V_0 = 62.0\ MeV$, $a_0 = 0.63\ fm$, $r_0 = 1.2\ fm$, $W_0 = 20.7\ MeV$, $a_i = 0.65\ fm$, and $r_i = 1.25\ fm$, which are listed in Table 3.1.

In (A) panel, the limit of all angles in coupled state is perfect agreement as well in panel (B) we obtained good match around barrier in coupled channel with measured data, so the barrier distribution as function of E_{cm} acceptable agreement in both coupled and no coupled channel above and under barrier**.**

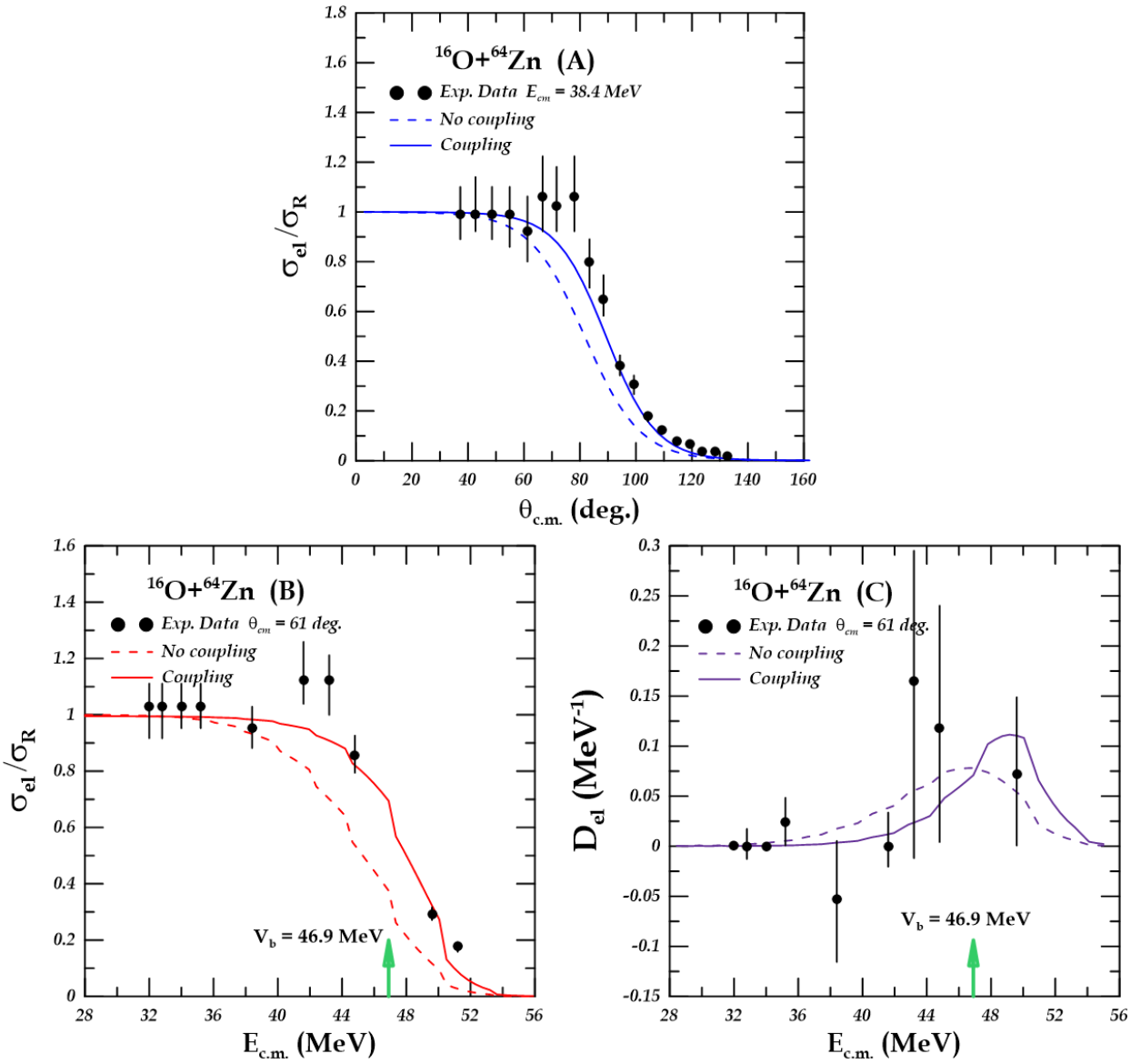

Figure 3.6 : Uncoupled channel and coupled channels calculations for $^{16}O+^{64}Zn$ system by dashed and solid curves respectively: **(A)** elastic scattering cross section with mass center angle, **(B)** elastic scattering cross section with energy center of mass, **(C)** elastic scattering barrier distribution with energy center of mass, the black circles are experimental data from Ref. [81].

3.2.7 ^{11}Be+^{209}Bi reaction

Figure 3.7 show the results of ^{11}Be+^{209}Bi reaction are taken the total differential cross section to the Rutherford differential cross section was determined with angle center of mass θ_{cm}.

The calculations have been performed for the nuclear system ^{11}Be+^{209}Bi where the projectile ^{11}Be is one neutron halo nucleus and the target ^{209}Bi is heavy ion, the Akyüz-Winther potential parameters $V_0 = 90.2\ MeV$, $a_0 = 0.63\ fm$, $r_0 = 1.2\ fm$, $W_0 = 130.1\ MeV$, $a_i = 0.77\ fm$, and $r_i = 1.29\ fm$, which are listed in Table 1. A good agreement between theoretical calculations and experimental data at limits of $\theta = 40^\circ - 75^\circ$ in coupled and uncoupled calculations, after $\theta = 90^\circ$, occurs obvious deviation from observed data. Due to the fact that the nucleus ^{11}Be is a halo and breakup channel has a major role in the rapid break of nucleus, which causes this deviation.

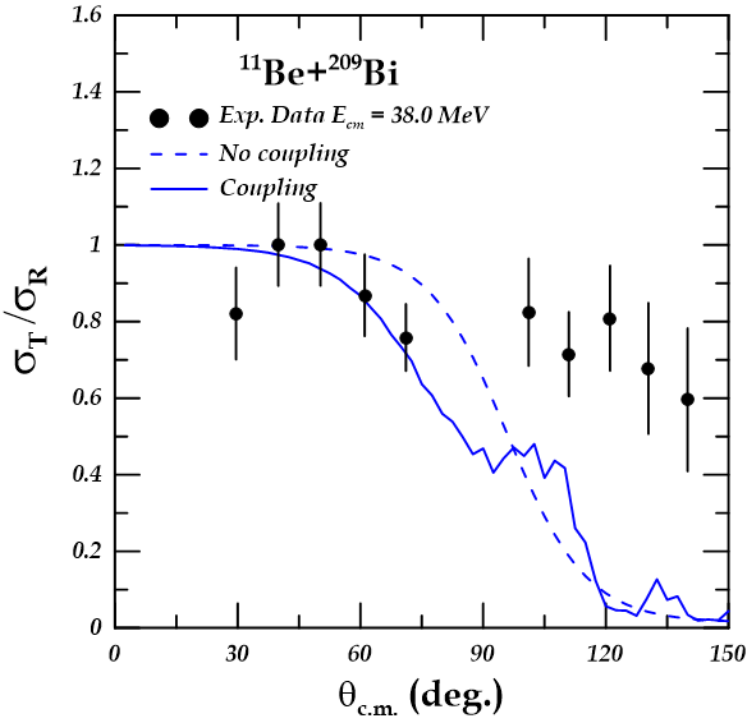

Figure 3.7: Uncoupled channel and coupled channels calculations for ^{11}Be+^{209}Bi system by red dashed and solid curves of total scattering cross section with the mass center angle, the black circles are experimental data from Ref. [82].

3.2.8 $^{32}S+^{208}Pb$ reaction

In the $^{32}S+^{208}Pb$ system, (see figure 3.8) the results of this reaction are taken the total cross section to the Rutherford cross section was determined with energy center of mass E_{cm} (panel A). The total scattering barrier distribution D_{el} was calculated with energy center of mass E_{cm} (in figure 3.8, panel B). The calculations have been performed for the nuclear system where the projectile ^{32}S is stable nucleus and the target ^{208}Pb is heavy ion, the Akyüz-Winther potential parameters $V_0 = 205.2\ MeV$, $a_0 = 0.63\ fm$, $r_0 = 1.1\ fm$, $W_0 = 68.4\ MeV$, $a_i = 0.56\ fm$, and $r_i = 1.34\ fm$. Agreement between theoretical calculations and experimental data is the best in no coupled state for total cross section from coupled state around Coulomb barrier. The number of experimental peaks in the distribution of the barriers corresponds to the number of the theoretical peaks, although the congruence is acceptable to some extent between results in coupled and uncoupled states.

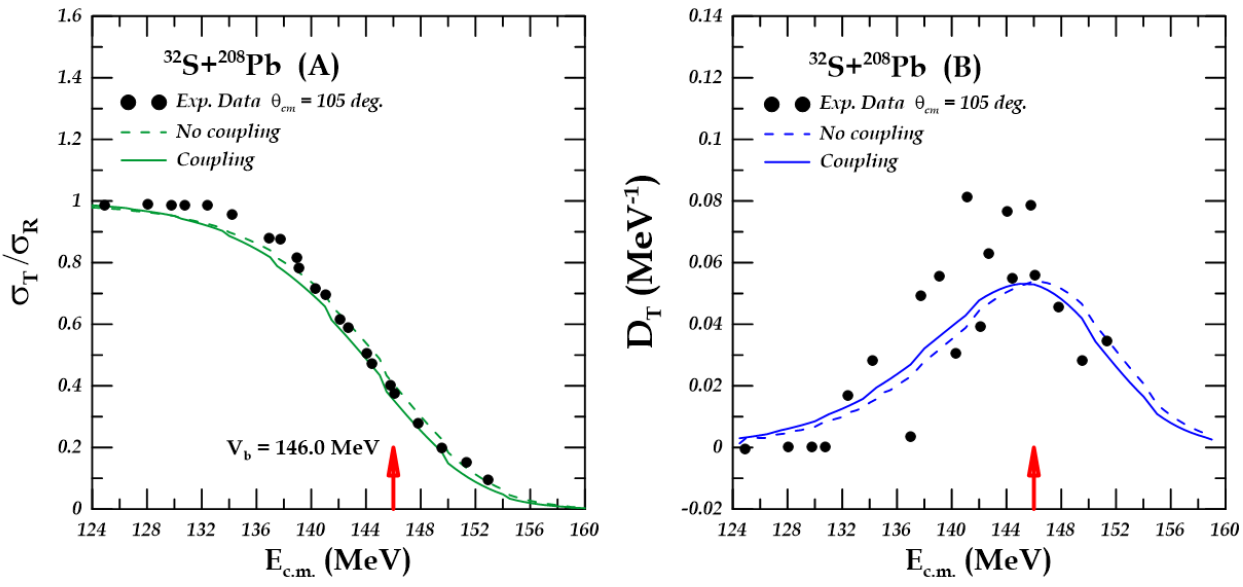

Figure 3.8 : Uncoupled channel and coupled channels calculations for $^{32}S+^{208}Pb$ system by dashed and solid curves respectively: **(A)** total scattering cross section with energy center of mass, **(B)** total scattering barrier distribution with the energy center of mass, the black circles are experimental data from Ref. [7].

3.3 Conclusions

There are deduce the following remarks based on the data and final conclusions presented in Tables (3.1) and Figures (3.1 to 3.8) for all systems researched in this thesis.:

1. The coupling of any the selected systems improved the calculations for elastic scattering and inelastic scattering.
2. We conclude that the breakup effect is very important for weakly bound projectiles, suppressed on heavy target nuclei above the Coulomb barrier, and, oppositely, is enhanced for some weakly bound projectiles at energies around the Coulomb barrier.
3. In $^{6}He+^{209}Bi$, we conclude measured values at incident energies down the Coulomb barrier that are identical with no-coupled and coupled calculations, and no obtaining measured values above barrier in experiment of the halo nucleus ^{6}He.
4. In $^{17}F+^{208}Pb$ and $^{11}Be+^{209}Bi$ systems, the major role of the breakup channel in halo nuclei causes the dispersion of the experimental data at different angles.
5. The stable projectiles in $^{16}O+^{64}Zn$ and $^{32}S+^{208}Pb$ systems, the total and elastic scattering are enhanced at energies down and above the Coulomb barrier.

3.4 Future Work

1. Using elastic and inelastic scattering with the double folding model (DFM) and dynamic polarization effective potential to perform the study and compare it with the present calculations.
2. Develop CC code to calculate cross-sections and barrier distributions for systems contain medium and heavy projectiles.

3. Using semiclassical approximation in scattering cross-sections and distribution calculations and its comparison with quantum mechanics calculations.
4. Studying new Halo and tightly bound nuclei on different targets nuclei at energies around barrier.
5. Develop CC code to calculate cross-sections and barrier distributions by using resonance theorem.

References

References

[1] V. Scuderi, A. Di Pietro, L. Acosta , F. Amorini, M. J. G. Borge, P. Figuera, M. Fisichella, L. M. Fraile, J. Gomez-Camacho, H. Jeppesen, M. Lattuada, I. Martel, M. Milin, A. Musumarra, M. Papa, M.G. Pellegriti, F. Perez-Bernal, R. Raabe, G. Randisi, F. Rizzo, D. Santonocito, G. Scalia, O. Tengblad, D. Torresi, A.M. Vidal, and M. Zadro, "Elastic scattering and direct reactions of the 1n halo ^{11}Be nucleus on ^{64}Zn near the barrier", Journal of Physics: Conference Series **381** (1), 012050 (2012).

[2] M. I. Ibrahim, M. Zamrun, and H. A. Kassim, "Analysis of the nuclear potential for heavy-ion systems through large-angle quasi-elastic scattering", Physical Review C **87** (2), 024611 (2013).

[3] V. Kovalchuk, "Quasi-Elastic Scattering of ^{6}He, ^{7}Be, and ^{8}B Nuclei by ^{12}C Nuclei", Russian Physics Journal **58** (8), 1134-1140 (2015).

[4] H. Timmers, J. R. Leigh, M. Dasgupta, D. J. Hinde, R. C. Lemmon, J. C. Mein, C. R. Morton, J.O. Newton, and N. Rowley, "Probing fusion barrier distributions with quasi-elastic scattering", Nuclear Physics A **584** (1), 190-204 (1995).

[5] Yu. Ts. Oganessian, F. Sh. Abdullin, P. D. Bailey, D. E. Benker, M. E. Bennett, S. N. Dmitriev, J. G. Ezold, J. H. Hamilton, R. A. Henderson, M. G. Itkis, Yu. V. Lobanov, A. N. Mezentsev, K. J. Moody, S. L. Nelson, A. N. Polyakov, C. E. Porter, A. V. Ramayya, F. D. Riley, J. B. Roberto, M. A. Ryabinin, K. P. Rykaczewski, R. N. Sagaidak, D. A. Shaughnessy, I. V. Shirokovsky, M. A. Stoyer, V. G. Subbotin, R. Sudowe, A. M. Sukhov, Yu. S. Tsyganov, V. K. Utyonkov, A. A. Voinov, G. K. Vostokin, and P. A. Wilk, "Synthesis of a new element with atomic number Z=117" Physical review letters, **104** (14), 142502 (2010).

[6] A. Mukherjee, D. Hinde, M. Dasgupta, K. Hagino, J. Newton, and R. Butt, "Failure of the Woods-Saxon nuclear potential to simultaneously

reproduce precise fusion and elastic scattering measurements", Physical Review C **75** (4), 044608 (2007).

[7] N. Wang, and W. Scheid, "Quasi-elastic scattering and fusion with a modified Woods-Saxon potential" Physical Review C **78** (1), 014607 (2008).

[8] K. Hagino, and K. Washiyama, "Probing internucleus potential with large-angle quasi-elastic scattering", in AIP Conference Proceedings **853** (1), 86-93 (2006).

[9] I. Dutt, "The role of surface diffuseness in heavy-ion fusion barriers studies", Nuclear Physics **57**, 470 (2012).

[10] J. R. Taylor, "Scattering Theory: The Quantum Theory on Nonrelativistic Collisions", John Wiley and Sons, Inc, (1972).

[11] E. Koelink, "Scattering theory", M.Sc. Thesis, Radbound Universiteit Nijmegen, (2009).

[12] H. P. gen. Schieck, "Nuclear Reactions An Introduction", Springer-Verlag Berlin Heidelberg, (2014).

[13] C. J. Joachain, "Quantum Collision Theory", North-Holland Publishing Company, (1975).

[14] W. Schroder and J. Huizenga, "Treatise on Heavy-ion Science", plenum, New York, London, (1984).

[15] J. Toke, and W. U. Schroder, "Excitation energy division in dissipative heavy-ion collisions", Annual Review of Nuclear and Particle Science **42** (1), 401-446 (1992).

[16] H. J. Arnikar, "Essentials of nuclear chemistry", New Age International (1995).

[17] S. B. Patel, "Nuclear physics", New Age International (1991).

[18] J. M. Blatt, and V. F. Weisskopf, "Theoretical Nuclear Physics", Dover Publications (1979).

[19] H. P. gen. Schieck, "Nuclear Reactions An Introduction", Springer-Verlag Berlin Heidelberg, (2014).

[20] J. Lilley, "Nuclear Physics, Principles and Applications", JohnWiley, Sons, Ltd, (2001).

[21] K. Riisager, D. V. Fedorov, and A. Jensen, "Quantum halos", Europhysics Letters **49** (5), 547 (2000).

[22] A. Jensen and M. Zhukov, "Few-body effects in nuclear halos", Nuclear Physics A **693** (1-2), 411-423 (2001).

[23] D. Fedorov, A. Jensen, and K. Riisager, "General properties of halos", Physics Letters B **312** (1-2), 1-5 (1993).

[24] A. Jensen and K. Riisager, Towards necessary and sufficient conditions for halo occurrence, Physics Letters B **480**, 39 (2000).

[25] C. B. Moon, "A nuclear physics program at the rare isotope beams accelerator facility in korea", AIP Advances **4** (4), 041001 (2014).

[26] I. Brida, "A Microscopic Hyper-spherical Model of Two-neutron Halo Nuclei", Michigan State University, Physics and Astronomy, (2009).

[27] P. Hansen, A. Jensen, and B. Jonson, "Nuclear halos", Annual Review of Nuclear and Particle Science **45** (CTHSP-95-08), 591 (1995).

[28] V. Rotival and T. Duguet, "New analysis method of the halo phenomenon in finite many-fermion systems: First applications to medium-mass atomic nuclei", Physical Review C **79**, 054308 (2009).

[29] S. V. S. Sastry and S. Santra, "Structure information from fusion barriers" Pramana **54** (6), 813-826 (2000).

[30] S. Santra, P. Singh, S. Kailas, A. Chatterjee, A. Shrivastava, and K.Mahata, "Coupled reaction channel analysis of elastic, inelastic, transfer, and fusion cross sections for $^{12}C+^{208}Pb$", Physical Review C **64** (2), 024602 (2001).

[31] T. J. Schuck, H. Timmers, and M. Dasgupta, "Investigation of the role of neutron transfer in the fusion of $^{32,34}S$ with ^{197}Au, ^{208}Pb using quasi-elastic scattering", Nuclear Physics A **712** (1-2), 14-22 (2002).

[32] I. Gontchar, D. Hinde, M. Dasgupta, and J. Newton, "Surface diffuseness of nuclear potential from heavy-ion fusion reactions", Nuclear Physics A **722**, C479-C483 (2003).

[33] A. Pakou, N. Alamanos, G. Doukelis, A. Gillibert, G. Kalyva, M. Kokkoris, S. Kossionides, A. Lagoyannis, A. Musumarra, C. Papachristodoulou, N. Patronis, G. Perdikakis, D. Pierroutsakou, E. C. Pollacco, and K. Rusek, "Elastic scattering of ^{7}Be + ^{28}Si at near-barrier energies", Physical Review C **95** (5), 054609 (2017).

[34] R. C. Johnson, "Adiabatic approximation for nucleus-nucleus scattering", AIP Conference Proceedings, American Institute of Physics **791** (1), 128-139 (2005).

[35] K. Washiyama, K. Hagino, and M. Dasgupta, "Probing surface diffuseness of nucleus-nucleus potential with quasielastic scattering at deep sub-barrier energies", Physical Review C **73** (3), 034607 (2006).

[36] K. Hagino, "Recent developments in quasi-elastic scattering around the Coulomb barrier", AIP Conference Proceedings **891** (1), 80-88 (2007).

[37] N. Wang and W. Scheid, "Quasi-elastic scattering and fusion with a modified Woods-Saxon potential", Physical Review C **78**, 014607 (2008).

[38] K. Hagino, "Fusion and Quasi-elastic scattering around the Coulomb barrier: determination of inter-nucleus potential", AIP conference proceedings **1120** (1), 3-8 (2009).

[39] A. Izadpanah, Causality principle and nuclear dispersion anomaly in the elastic scattering for $\alpha+^{12}$C system. Chinese Physics C **34** (12), 1842 (2010).

[40] W. H. Long, and C. A. Bertulani, "Nucleus-nucleus interaction between boosted nuclei", Physical Review C **83**(2), 024907 (2011).

[41] S. Yusa, K. Hagino, and N. Rowley, "Quasi-elastic scattering in the ^{20}Ne+^{90,92}Zr reactions: Role of noncollective excitations", Physical Review C **88**, 054621 (2013).

[42] E. C. Pinilla, and P. Descouvemont, "Microscopic description of ^{7}Li in ^{7}Li+^{12}C and ^{7}Li+^{28}Si elastic scattering at high energies", Physical Review C **89** (5), 054615 (2014).

[43] V. I. Kovalchuk, "Quasi-Elastic Scattering of ^{6}He, ^{7}Be, and ^{8}B Nuclei by ^{12}C Nuclei", Russian Physics Journal **58** (8), 1134-1140 (2015).

[44] J. P. Fernández-García, A. Di Pietro, P. Figuera, M. Fisichella, M. Lattuada, A. M. Moro, A. Musumarra, M. G. Pellegriti1, V. Scuderi1, D. Torresi and M. Zadro, "Effects of coupling to breakup channels in reactions induced by weakly bound and halo nuclei", EPJ Web of Conferences **117**, 06012 (2016).

[45] N. Burtebayev, S. B. Sakuta, A. K. Morzabayev Zh. K. Kerimkulov, N. Amangeldi, A.A. Temerbayev B. Mauyey, Ye. Koka, and A.S. Aimaganbetov, "Elastic Scattering of ^{15}N Ions by ^{16}O at the Energy 11.59 MeV", Acta Physica Polonica B **48** (3), 495 (2017).

[46] S. R. Mokhtar, A. A. Ibraheem, E. Abdel-Rahman, and M. El-Azab Farid, "Investigation of the ^{6}Li+^{40}Ca elastic scattering using different folding models", The European Physical Journal A **54** (12), 1-9 (2018).

[47] Q. J. Tarbool, K. S. Jassim, and A. A. Abojassim, "Surface diffuseness parameter with quasi-elastic scattering for some heavy-ion systems", International Journal of Nuclear Energy Science and Technology **13** (2), 110-119 (2019).

[48] A. J. Hassan, and K. S. Jassim, "Effect of Surface Diffuseness Parameter on Quasi-elastic Scattering Calculations for ^{6}He+^{64}Zn, ^{7}Li+^{64}Zn, and ^{8}Li+^{90}Zr Systems", NeuroQuantology **18** (9), 40 (2020).

[49] K. Wang, Y. Y. Yang, A. M. Moro, V. Guimarães, Jin Lei, D. Y. Pang, F. F. Duan, J. L. Lou, J. C. Zamora, J. S. Wang, Z. Y. Sun, H. J. Ong, X. Liu, S. W. Xu, J. B. Ma, P. Ma, Z. Bai, Q. Hu, X. X. Xu, Z. H. Gao, G. Yang, S. Y. Jin, Y. H. Zhang, X. H. Zhou, Z. G. Hu, and H. S. Xu, "Elastic

scattering and breakup reactions of the proton drip-line nucleus ^{8}B on ^{208}Pb at 238 MeV", Physical Review C **103**(2), 024606 (2021).

[50] K. Hagino, N. Rowley, and A. Kruppa, "A program for coupled-channel calculations with all order couplings for heavy-ion fusion reactions" Computer Physics Communications **123**, 143-152 (1999).

[51] G. R. Satchler and W. G. Love, "Folding model potentials from realistic interactions for heavy-ion scattering" Physics Reports **55**, 183-254 (1979).

[52] K. Hagino, T. Takehi, A. Balantekin, and N. Takigawa, "Surface diffuseness anomaly in heavy-ion potentials for large-angle quasielastic scattering", Physical Review C **71** (4), 044612 (2005).

[53] M. Dasgupta, D. Hinde, J. Newton, and K. Hagino, "The nuclear potential in heavy-ion fusion", Progress of Theoretical Physics Supplement **154**, 209-216 (2004).

[54] C. Dfold, Universität Tübingen, unpublished (1989).

[55] D. J. Griffiths "Introduction to Quantum Mechanics", Pearson Education International, 2nd edition (2005).

[56] P. Fröbrich, and R. Lipperheide, "Theory of Nuclear Reactions", Oxford University Press, New York, (1996).

[57] R. D. Woods, and D. S. Saxon, "Diffuse surface optical model for nucleon-nuclei scattering", Physical Review **95** (2), 577 (1954).

[58] H. Feshbach, C. E. Porter, and V. F. Weisskopft, "The formation of a compound nucleus in neutron reactions", Physical Review **90** (1), 166 (1953).

[59] H. Feshbach, "A unified theory of nuclear reactions II", Annals of Physics **19** (2), 287-313 (1962).

[60] H. Feshbach, "Unified theory of nuclear reactions", Annals of Physics **5** (4), 357-390 (1958).

[61] H. Feshbach, D. C. Peasly and V. F. Weisskopft, "On the scattering and absorption of particles by atomic nuclei", Physical Review **71** (3), 145 (1947).

[62] M. Kamimura, M. Yahiro, Y. Iseri, Y. Sakuragi, H. Kameyama, and M. Kawai, "Coupled-channels theory of breakup processes in nuclear reactions", Progress of Theoretical Physics Supplements, 89 (1), (1986).

[63] N. Austern, Y. Iseri, M. Kamimura, M. Kawai, G. Rawitscher, and M. Yahiro, "Continuum-discretized coupled-channels calculations for three-body models of deuteron-nucleus reactions", Physical Report **154** (3), 125-204 (1987).

[64] M. Giles, "Non-reflecting boundary conditions for the Euler equations: Computational Fluid Dynamics Laboratory", Department of Aeronautics and Astronautics, Massachusetts Institute of Technology, (1988).

[65] A. Balantekin, A. DeWeerd, and S. Kuyucak, "Relations between fusion cross sections and average angular momenta", Physical Review C **54**, 1853 (1996).

[66] K. Hagino, and N. Takigawa, "Subbarrier fusion reactions and many-particle quantum tunneling", Progress of theoretical physics **128**, 1061-1106 (2012).

[67] H. S. Bosch and G. Hale, Improved formulas for fusion cross-sections and thermal reactivities, Nuclear fusion **32**, 611 (1992).

[68] H. Timmers, J. R. Leigh, M. Dasgupta, D. J. Hinde, R. C. Lemmon, J. C. Mein, C. R. Morton, J.O. Newton, and N. Rowley, Nuclear Physics A **584**, 190 (1995).

[69] D. M. Brink, "Semi-Classical Methods for Nucleus-Nucleus Scattering", Cambridge University Press, Cambridge, England, (1985).

[70] S. Landowne and H. H. Wolter, "On sub-Coulomb heavy-ion scattering and the problem of nuclear absorption", Nuclear Physics A **351** (1), 171-188 (1981).

[71] D. M. Brink, and G. R. Satchler, "The role of the attractive nuclear potential in determining reaction cross sections", Journal of Physics G: Nuclear Physics **7** (1), 43 (1981).

[72] A. T. Kruppa, P. Romain, M. A. Nagarajan, and N. Rowley, "Effect of multiphonon coupling on heavy-ion fusion", Nuclear Physics A **560** (3), 845-862 (1993).

[73] D. R. Otomar, J. Lubian, and P.R.S. Gomes, "Investigation of breakup effects on ^{6}Li+^{144}Sm scattering by means of CDCC calculations", The European Physical Journal A **46** (2), 285-289 (2010).

[74] L. F. Canto, P. R. S. Gomes, R. Donangelo, J. Lubian, and M. S. Hussein, "Recent developments in fusion and direct reactions with weakly bound nuclei", Physics Reports **596**, 1-86 (2015).

[75] J. M. Figueira, J. F. Niello, A. Arazi, O. A. Capurro, P. Carnelli, L. Fimiani, and P. R. S. Gomes, "Energy dependence of the optical potential of weakly and tightly bound nuclei as projectiles on a medium-mass target", Physical Review C **81** (2), 024613 (2010).

[76] M. A. G. Alvarez, M. Rodríguez-Gallardo, J. P. Fernández-García, J. Casal, and J. A. Lay, "Systematic calculations of reactions with exotic and stable nuclei to establish a unified theoretical approach", Physical Review C **103** (5), 054614 (2021).

[77] J. P. Fernández-García, M. A. G. Alvarez, A. M., Moro, and M. Rodríguez-Gallardo, "Simultaneous analysis of elastic scattering and transfer/breakup channels for the ^{6}He+ ^{208}Pb reaction at energies near the Coulomb barrier", Physics Letters B **693** (3), 310-315 (2010).

[78] C. H. Rong, J. Rangel, Y. S. Wu, G. L. Zhang, G. X. Zhang, C. J. Lin, E. N. Cardozo, X. Y. Wang, L. Yang, N. R. Ma, D. X. Wang, L. J. Sun, H. M. Jia, F. Yang, J. S. Wang, Y. Y. Yang, J. B. Ma, P. Ma, Z. Bai, S. W. Xu, F. F. Duan, X. B. Qin, H. M. Zhao, and J. Lubian, "Study of quasi-elastic

scattering of $^{17}F+^{208}Pb$ at energies around Coulomb barrier", The European Physical Journal A, **57** (4), 1-18 (2021).

[79] C. Beck, N. Rowley, P. Papka S. Courtin, M. Rousseau, F. A. Souza, N. Carlin, R. Liguori Neto, M. M. de Moura, M. G. Del Santo, A. A. P. Suaide, M. G. Munhoz, E. M. Szanto, A. Szanto de Toledo, N. Keeley, A. Diaz-Torres, and K. Hagino, "Reaction mechanisms for weakly-bound, stable nuclei and unstable, halo nuclei on medium-mass targets", Nuclear Physics A, **834** (1-4), 440c-445c. (2010).

[80] C. Beck, N. Keeley, and A. Diaz-Torres, "Coupled-channel effects in elastic scattering and near-barrier fusion induced by weakly bound nuclei and exotic halo nuclei", Physical Review C, **75** (5), 054605 (2007).

[81] P. R. S. Gomes, M. D. Rodr´ıguez, G. V. Mart´ı, I. Padron, L. C. Chamon, J. O. Fern´andez Niello, O. A. Capurro, A. J. Pacheco, J. E. Testoni, A. Arazi, M. Ram´ırez, R. M. Anjos, J. Lubian, R. Veiga, R. Liguori Neto, E. Crema, N. Added, C. Tenreiro, and M. S. Hussein, "Effect of the breakup on the fusion and elastic scattering of weakly bound projectiles on ^{64}Zn", Physical Review C **71** (3), 034608 (2005).

[82] M. Mazzocco, C. Signorini, M. Romoli, A. De Francesco, M. Di Pietro, E. Vardaci, K. Yoshida, A. Yoshida, R. Bonetti, A. De Rosa, T. Glodariu, A. Guglielmetti, G. Inglima, M. La Commara, B. Martin, D. Pierroutsakou, M. Sandoli, F. Soramel, L. Stroe, R. Kanungo, N. Khai, T. Motobayashi, T. Nomura, T. Ishikawa, H. Ishiyama, S. Jeong, H. Miyatake, M. H. Tanaka, I. Sugai, and Y. Watanabe, "Scattering of ^{11}Be halo nucleus from ^{209}Bi at the Coulomb barrier", The European Physical Journal A-Hadrons and Nuclei, **28** (3), 295-299 (2006).

الخلاصة

في هذه الرسالة، الدراسة العلمية لالية الاستطارة تم تنفيذها لحساب المقاطع العرضية للاستطارة الكلية (σ_T/σ_R) او المرنة (σ_{el}/σ_R) نسبة الى المقاطع العرضية لرذرفورد مع توزيع حاجز كولوم $(D_{el}$ or $D_T)$ (MeV^{-1}) لنوى مستقرة وغير مستقرة في العديد من الأنظمة هي : $^{6}\mathrm{He}+^{208}\mathrm{Pb}$, $^{17}\mathrm{F}+^{208}\mathrm{Pb}$, $^{7}\mathrm{Be}+^{58}\mathrm{Ni}$, $^{7}\mathrm{Li}+^{59}\mathrm{Co}$, $^{6}\mathrm{Li}+^{59}\mathrm{Co}$, $^{16}\mathrm{O}+^{64}\mathrm{Zn}$, $^{32}\mathrm{S}+^{208}\mathrm{Pb}$, and $^{11}\mathrm{Be}+^{209}\mathrm{Bi}$.

وجدنا أن أفضل طريقة ملائمة للأستطارة في وصف الجهد النووي البصري باستخدام شكل وود ساكسون Wood-Saxon (WS) الذي يحوي بارامترات الجزء الحقيقي والخيالي وهي العمق، نصف القطر ومعامل انتشار السطح النووي. القيم الافضل لبارامترات الجهد البصري نفذت بطريقة فت جيدة للحسابات النظرية مع القيم العملية. هذه الدراسة استندت على نظرية Alder and Winther التي افترضت بالاصل لتعالج التهيجات الكولومية للانوية وتدعى طريقة القنوات المقترنة المتقطعة- المستمرة CDCC.

اقتران قنوات التفاعل مع قناة التفكك على الحسابات تم تنفيذها بواسطة برنامج CC-SCT يمثل النسخة الاحدث لكود CC الذي برمج بلغة فورتران. برنامج فرعي كتب بلغة فورتران في حساب توزيع حاجز الاستطارة D_{el} or D_T بطريقة فرق نقطتين عددية. البرنامج الفرعي نفذت ببرنامج CC-SCT للنتائج النظرية والعملية.

حسابات النسبة بين المقاطع العرضية للاستطارة الى مقاطع استطارة رذرفورد كدالة لمركز الزاوية θ_{cm} ودالة لمركز الطاقة E_{cm} بالإضافة الى حساب توزيع الاستطارة المرنة كدالة للطاقة D_{el} في حالات الاقتران وعدم الاقتران. كل الحسابات في توافق جيد مع القيم العملية.

جمهورية العراق

وزارة التعليم العـــالي والبحث العلـمي
جامـــعة بابـــل
كليـــة التربية للعلوم الصرفة
قســـم الفيزيـــاء

آلية تفاعلات الأستطارة لبعض النوى المستقرة وغير المستقرة على أهداف متوسطة وثقيلة الكتلة

رسالة مقدمة

إلى مجلس كلية التربية للعلوم الصرفة في جامعة بابل

وهي جزء من متطلبات نيل درجة الماجستير

في التربية / الفيزياء

من قبل الطالبة

زينب حافظ موسى سبيل

بكالوريوس تربية فيزياء

(جامعة بابل 2009 م)

بأشراف

أ. م. د. فاطمة محمد حسين

كلية التربية للعلوم الصرفة

قسم الفيزياء

1444 هـ

2022 م